Cooper, A.K., O'Brien, P.E., and Richter, C. (Eds.)
Proceedings of the Ocean Drilling Program, Scientific Results Volume 188

13. Data Report: HiRISC (High-Resolution Integrated Stratigraphy Committee) Pliocene–Pleistocene Interval, 0–50 mbsf, at ODP Leg 188 Site 1165, Prydz Bay, Antarctica[1]

Detlef A. Warnke,[2] Carl Richter,[3] Fabio Florindo,[4] John E. Damuth,[5] William L. Balsam,[5] Kari Strand,[6] Mattiina Ruikka,[6] Juho Juntila,[6] Kevin Theissen,[7] and Patrick Quilty[8]

ABSTRACT

During Ocean Drilling Program Leg 188 to Prydz Bay, East Antarctica, several of the shipboard scientists formed the High-Resolution Integrated Stratigraphy Committee (HiRISC). The committee was established in order to furnish an integrated data set from the Pliocene portion of Site 1165 as a contribution to the ongoing debate about Pliocene climate and climate evolution in Antarctica. The proxies determined in our various laboratories were the following: magnetostratigraphy and magnetic properties, grain-size distributions (granulometry), near-ultraviolet, visible, and near-infrared spectrophotometry, calcium carbonate content, characteristics of foraminifer, diatom, and radiolarian content, clay mineral composition, and stable isotopes. In addition to the HiRISC samples, other data sets contained in this report are subsets of much larger data sets. We included these subsets in order to provide the reader with a convenient integrated data set of Pliocene–Pleistocene strata from the East Antarctic continental margin. The data are presented in the form of 14 graphs (in addition to the site map). Text and figure captions guide the reader to the original data sets. Some preliminary interpretations are given at the end of the manuscript.

[1]Warnke, D.A., Richter, C., Florindo, F., Damuth, J.E., Balsam, W.L., Strand, K., Ruikka, M., Juntila, J., Theissen, K., and Quilty, P., 2004. Data report: HiRISC (High-Resolution Integrated Stratigraphy Committee) Pliocene–Pleistocene interval, 0–50 mbsf, at ODP Leg 188 Site 1165, Prydz Bay, Antarctica. *In* Cooper, A.K., O'Brien, P.E., and Richter, C. (Eds.), *Proc. ODP, Sci. Results,* 188, 1–38 [Online]. Available from World Wide Web: <http://www-odp.tamu.edu/publications/188_SR/VOLUME/CHAPTERS/014.PDF>. [Cited YYYY-MM-DD]
[2]Department of Geological Sciences, California State University, Hayward, 25800 Carlos Bee Boulevard, Hayward CA 94542, USA.
dwarnke@csuhayward.edu
[3]University of Louisiana at Lafayette, PO Box 44530, Lafayette LA 70504, USA.
[4]Istituto Nazionale di Geofisica e Vulcanologia, Via di Vigna Murata 605, I-00143 Rome, Italy.
[5]Department of Geology, University of Texas at Arlington, PO Box 19049, 500 Yates Street, Room 107, Arlington TX 76019, USA.
[6]Thule Institute, University of Oulu, Linnanmaa, PO Box 7300, FIN-90014, Finland.
[7]Geological and Environmental Sciences, Stanford University, Building 320, Room 118, Stanford CA 94305-2215, USA.
[8]School of Earth Sciences, University of Tasmania, Sandy Bay Campus, GPO Box 252-79, Hobart TAS 7050, Australia.

Initial receipt: 10 February 2003
Acceptance: 8 August 2003
Web publication: 30 January 2004
Ms 188SR-015

INTRODUCTION

Site 1165 was drilled on Wild Drift, a thick contourite deposit on the continental rise off Prydz Bay, East Antarctica (64°22.77′S, 67°13.14′E; 3537 m water depth) to a total depth of 999.1 meters below seafloor (mbsf) (Fig. F1) (O'Brien, Cooper, Richter, et al., 2001). Terrigenous and hemipelagic sediments of early Miocene–Quaternary age were recovered including a thick section of contourites. Of special interest to several members of the shipboard science party and their colleagues is the uppermost sediment column between 0 and 50 mbsf, which consists of a section of hemipelagic and pelagic Pliocene–Pleistocene sediments. The stability of the Antarctic ice sheets during the Pliocene—particularly the Gauss Chron (C2An; 2.581–3.580 Ma)—was and is the subject of much debate (Robin, 1988; Hodell and Warnke, 1991; Webb and Harwood, 1991; Hambrey and Barrett, 1993; Quilty, 1993, 1996; Kennett and Hodell, 1993; Warnke et al., 1996; Burckle et al., 1996), mainly based on studies in the Ross Sea/Transantarctic Mountains region. There are several competing ideas concerning the size and fluctuations of the Antarctic ice sheets. These range from minimal size to greatly expanded ice volume, from a perennially frozen landscape to one undergoing active modification, from survival of southern beech trees on Antarctica to environments not supporting higher land plants at all, and so on. Lately, there seems to have been some convergence of ideas among some participants in this debate to the effect that expansions of the ice sheet across the continental shelves took place during brief intervals of time (Whitehead et al., 2001; Bart, 2001). On the topic of ice volume reduction and retreat of the grounding line, there is less agreement. It is not our intention to review the entire debate here. The reader is referred to the above publications. A recent description of the problem, from a "conservative" point of view, is provided by Murphy et al. (2002).

For the entire interval of Antarctic cryospheric evolution, the Pliocene, particularly the early late Pliocene (Piacenzian) is probably the interval that is least understood and most widely debated. The reason for this wide range of ideas is the fact that different investigators used completely different proxies as the bases for their interpretations, and it was inherently difficult to reconcile the contrasting evidence provided by these different proxies.

During Leg 188, it became clear that shipboard scientists were positioned on all sides of the debate. We realized that Site 1165 contained a reasonably well preserved (for an Antarctic margin setting) Pliocene record, particularly the Gauss normal polarity chron including the Kaena (C2An.1r; 3.040–3.110 Ma) and Mammoth (C2An.2r; 3.220–3.330 Ma) Subchrons, which are well identified at this site (timescale of Berggren et al., 1995; Shipboard Scientific Party, 2001). This interval is important because it contains the PRISM2 (Middle Pliocene Paleoenvironmental Reconstruction) time slab (3.15–2.85 Ma) described by Dowsett et al. (1999). The global ice volume and, consequently, the sea level stand during this period of past global warmth is important because both Pliocene ice volume and sea level stand may provide an indication of how Earth may respond to future global warming (Dowsett et al., 1999). Because of the importance of this possibility, we organized the "High-Resolution Integrated Stratigraphy Committee" (HiRISC), whose members reflect various nuances of the ongoing Pliocene debate. The goal of this committee is to provide proxy data sets of various parame-

F1. Location map, p. 20.

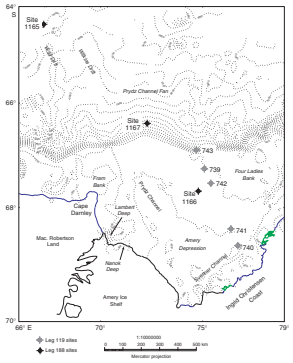

ters throughout this interval that can be used by all investigators in their participation in the Pliocene debate. It is not the aim of the committee to "solve" the Pliocene problem but rather to provide facts that can be used by all as they see fit. Sampling was done at 10-cm intervals (although in places the sampling interval was variable), and most samples were shared by committee members. Other samples were taken where needed near the "main samples."

The proxies that were determined in our various laboratories were the following: magnetostratigraphy and magnetic properties, grain-size distributions (granulometry), near-ultraviolet/visible/near-infrared (NUV/VIS/NIR) spectrophotometry, calcium carbonate content, characteristics of foraminifer, diatom, and radiolarian content, clay-mineral composition, and stable isotopes. In addition to the HiRISC samples, other data sets contained in this report are subsets of much larger data sets. We included these subsets in order to provide the reader with a convenient integrated data set of Pliocene–Pleistocene strata from the East Antarctic continental margin.

METHODOLOGIES

Magnetostratigraphy

The bulk of the remanence measurements made during Leg 188 were carried out using a 2G Enterprises (model 760-R) pass-through cryogenic magnetometer equipped with pickup coils that enable measurement of the magnetic signal over an interval of ~8 cm (Shipboard Scientific Party, 2001). Natural remanent magnetization (NRM) was routinely measured before and after alternating-field (AF) demagnetization on all archive-half core sections at 4-cm intervals. Time constraints permitted analysis with only two or three AF demagnetization steps at 10-, 20-, and 30-mT peak values for most of the core sections. The low maximum peak AFs ensured that the archive halves remained useful for shore-based paleomagnetic studies. In a few intervals, the presence of strong magnetic overprints necessitated progressive demagnetization of the archive halves up to 60–80 mT. Measurements at the end of each core section and those within intervals of drilling-related core deformation and in the vicinity of obvious metamorphic and/or igneous pebbles were removed during data processing.

Discrete samples (standard 8-cm^3 plastic cubes) were collected from the working halves of the cores at ~1-m intervals and were analyzed to verify the reliability of the whole-core measurements on the archive core halves. If possible, these samples were taken from fine-grained horizons and sampling was adjusted to avoid intervals with drilling-related core deformation and pebbles. Most discrete samples were AF demagnetized at 10, 20, 30, 40, 50, 60, 70, and 80 mT using the in-line demagnetizer installed on the 2G Enterprises pass-through cryogenic magnetometer on the ship. A subset of samples was thermally demagnetized on the ship using a Schonstedt TSD-1 oven. All of the samples subjected to thermal demagnetization were measured at steps of 20°, 100°, 200°, 300°, 330°, 360°, 400°, 500°, 550°, 600°, 650°, and 700°C. The magnetic susceptibility was measured after each heating step to monitor for thermal alteration of magnetic minerals.

The lack of azimuthal orientation for these cores does not pose a problem for determination of paleomagnetic polarity in our magnetostratigraphic studies because the geomagnetic field at the latitude of

Site 1165 (64.4°S) has a steep inclination (±76.5°, assuming a geocentric axial dipole field). The paleomagnetic inclinations were determined using the 20- to 30-mT steps from the long-core measurements and using principal component analysis (Kirschvink, 1980) for data from multiple demagnetization steps for discrete samples. The maximum angular deviation (MAD) was calculated to provide an estimate of the precision for each best-fit line. Samples were only included in this study if MAD values were <10°.

Mineral magnetic analyses were conducted on a set of representative discrete samples after they had been subjected to AF demagnetization in order to estimate downcore variations in the composition, concentration, and grain size of magnetic minerals. Low-field magnetic susceptibility (*k*) was routinely measured for all the discrete samples using a Bartington Instruments MS2 magnetic susceptibility meter. Further analyses were made on a selected subset of discrete samples. These analyses included (1) stepwise acquisition of an isothermal remanent magnetization (IRM) in fields up to 1.3 T; (2) determination of the coercivity of remanence (Bcr) and S-ratio (–IRM [–0.3 T]/IRM [1.3 T]) by progressively applying increasing backfields up to 300 mT after application of a forward-field IRM at 1.3 T; and (3) anhysteretic remanent magnetizations (ARMs) imparted with a 100-mT AF and a 0.05-mT direct current (DC) bias field. For a few samples, we also carried out a stepwise thermal demagnetization of a composite IRM (Lowrie, 1990) at steps of 20°, 100°, 200°, 300°, 330°, 360°, 400°, 500°, 550°, 600°, 650°, and 700°C. Fields of 1.3, 0.5, and 0.12 T were applied along the x-, y-, and z-axes of samples to distinguish between high-, intermediate-, and low-coercivity magnetic phases, respectively. Temperature dependence of magnetic susceptibility was also measured for selected samples from room temperatures up to 700°C, using a furnace-equipped Kappabridge KLY-3 magnetic susceptibility meter (Hrouda, 1994).

Granulometry

Grain-size separations were carried out using standard methods, as described in Allen and Warnke (1991). The >63-µm fraction was dry-sieved into the 63- to 150-µm, 150-µm to 2-mm, and >2-mm fractions. For the purposes of this report, the 63- to 150-µm and 150-µm to 2-mm fractions were combined in the accompanying graphs. Analyses of samples in the depth range of 0–15 mbsf were performed at Stanford University. Analyses of samples in the interval 15–50 mbsf were carried out at California State University, Hayward.

Calcium Carbonate

For the HiRISC section in Hole 1165B, we determined the calcium carbonate content for closely spaced (~10 cm) samples provided by HiRISC. We used the vacuum gasometric technique of Jones and Kaiteris (1983) to determine weight percent calcium carbonate content for all HiRISC samples in Hole 1165B from 0 to 54 mbsf (Fig. **F2**) (see **Damuth and Balsam,** their table **T1,** this volume, for sample intervals and carbonate values). With this technique, a small (~0.25 g) powdered sample is digested in concentrated phosphoric acid under vacuum and the pressure generated by the release of CO_2 is recorded on a vacuum gauge. Weight percent $CaCO_3$ is calculated by relating the pressure increase in the sample to the pressure increase in reagent carbonate after correcting for temperature and pressure. The Jones and Kaiteris (1983)

F2. Calcium carbonate content and brightness, p. 21.

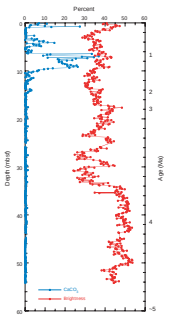

technique has an accuracy of about ±1%. As with most techniques used to determine carbonate, the Jones and Kaiteris (1983) technique combines both polymorphs of $CaCO_3$, calcite, and aragonite, as well as carbonate from biogenic and nonbiogenic sources. In most marine settings dolomite is not a significant contributor to the carbonate component. The Pleistocene and uppermost Pliocene sediments in this section (0–10 mbsf) show wide fluctuations in carbonate content, ranging from 0 to 37 wt%. Below 10 mbsf the carbonate content is generally zero and rarely rises to a few weight percent. Most of the values in this interval are <0.4 wt% and are below the accuracy of the instrument.

NUV/VIS/NIR Spectral Analysis

NUV/VIS/NIR spectral data were measured from all samples taken from Sites 1165 and 1167 with our laboratory-grade PerkinElmer Lambda 6 spectrophotometer at the University of Texas at Arlington (UTA) (**Damuth and Balsam,** this volume). Sample preparation followed the procedures described by Balsam and Deaton (1991). Reflectance spectrophotometers such as ours are designed to scan different wavelengths of light reflected from a sample's surface and record the intensity of that reflected light relative to a white standard (e.g., barium sulfate) used to set the 100% reflectance level. The PerkinElmer Lambda 6 spectrophotometer uses a reflectance sphere, which is a diffuse reflectance attachment that allows total reflectance measurements to be made from the near infrared (250 nm) through the visible into the near ultraviolet (850 nm). The Lambda 6 contains two light sources, a tungsten lamp for 350–850 nm and a deuterium lamp for 250–350 nm, a moving grating (to separate light into different wavelengths), and a photomultiplier tube (to measure the intensity of light reflected from the sample surface). Data from the spectrophotometer are recorded directly on a floppy disk at 1-nm intervals from 250 to 850 nm, the analytical range of the Lambda 6 in the reflectance mode. Samples were analyzed using a slit width of 2 nm at a scan rate of 600 nm/min. Details and data tables are presented in the companion paper by **Damuth and Balsam** (this volume; their table **T2**). In the accompanying figures, we display curves showing brightness downhole as *percent brightness*, which is simply brightness values rescaled to 100%.

Stable Isotopic Analyses

Left-coiling foraminifers of the planktonic species *Neogloboquadrina pachyderma* (s.) dominate surface sediment foraminifer assemblages in polar regions (Bé, 1977) and are used widely in paleoclimatic and paleoceanographic studies (e.g., Mackensen et al., 1989; Charles and Fairbanks, 1990; Hodell, 1993). At Site 1165, *N. pachyderma* (s.) composes the large majority of preserved foraminifers from the Pliocene–Pleistocene section and is present in sufficient numbers for stable isotopic analysis in the upper 16.36 mbsf. Foraminifers are generally well preserved, although there is evidence of dissolution (broken tests, holes in tests, etc.) in some samples that may affect their stable isotopic values.

Methods

Sediment samples, taken at 20-cm intervals, were soaked in a dilute Calgon solution, wet sieved, and separated into several fractions (>2 mm, 150 µm–2 mm, 63–150 µm, and <63 µm). All fractions were dried

in an oven at 50°C. *N. pachyderma* (s.) specimens were picked from the >150-µm fraction. Samples in the upper 16.36 mbsf contained sufficient foraminifers for stable isotopic measurements. All remaining samples (to 50 mbsf) were either barren of foraminifers or, in rare cases, had poorly preserved foraminifers that were deemed unsuitable for analysis. All measurements were made at the Stanford University Stable Isotope Laboratory. Analytical methods and precision are described in **Theissen et al.** (this volume).

Clay Mineral Analyses

X-ray diffraction (XRD) was performed on oriented clay samples. The sediment samples were first decomposed by ultrasonic vibration then centrifuged for 1 min to suspend clay minerals (<2 µm). Samples were then concentrated by centrifugation for 15 min. The separated clay minerals were treated by standard methods: air-dried, glycolated, and heated following the technique described by Hardy and Tucker (1988). Clays were fed to the XRD (Siemens D 5000) at angles from 2° to 32°2θ (0.02°θ 2/s) immediately after the treatments. The four principal clay mineral groups have basal spacings at 7 Å (kaolinite and chlorite), 10 Å (illite), 12–15 Å (smectite), and 14 Å (chlorite), and mixed-layer minerals give intermediate or higher values. Ethylene glycol treatment was used to separate smectite from chlorite. Kaolinite collapses when heated. In this study chlorite (004) was identified at 3.54 Å and kaolinite (002) at 3.58 Å, and this proportion was used to calculate quantities of kaolinite and chlorite from the joint peak at 7 Å. MacDiff software version 4.25 (Petschick, 2001) was used to quantify clay minerals, which were then used to calculate percentages using weighting factors (Biscaye, 1964). Since no internal standards were used, the exact accuracy is not known; however, the quantitative analyses justify interpretations of fluctuations which are around ± 2%.

Foraminifer Analyses

Materials and Methods

The section studied is that contained in intervals 188-1165B-1H-1, 0.17–0.21 cm, through 2H-6, 0.66–0.69 cm (0.17–14.96 mbsf). The lower depth limit is that below which foraminifers are virtually absent. The following should be considered an amplification of analyses contained in **Quilty** (this volume).

This study is designed to detect changes in distribution of foraminifers and to relate these to other parameters measured as part of the HiRISC project. Although some quantification is attempted, this should not be interpreted as a productivity signal, as it probably is more influenced by carbonate dissolution patterns than by productivity.

The site appears to lie within the Antarctic Divergence Zone where currents are westerly flowing, but the oceanography probably has varied considerably within the timescale under study and it is possible that, at different times, the area has been both north and south of the divergence.

Samples studied are those in the 150-µm to 2-mm mesh range, prepared by K. Theissen at Stanford University, California. Sample numbers included on Table **T1** are those supplied by Ocean Drilling Program (ODP).

T1. Foraminifers at 0–15 mbsf, Site 1165, p. 35.

As many samples are very highly dominated by *N. pachyderma* (Ehrenberg), all samples were split to smaller, more manageable, volumes. All foraminifers were manually separated from the smaller subsamples, glued down on separate slides, counted, and identified. Data were compiled in the accompanying table (Table T1), and basic analyses were carried out.

Factors affecting the accuracy of counts include human error and, especially, the effects of dissolution and breakage, which influence the content of fragmented specimens, leading to occasional double counting or even noncounting when fragments pass through the finer sieve size.

Whereas the object of the study concerned the foraminifers, records were kept of other aspects of the residues, such as dominant components and presence or absence of trace amounts of sponge or echinoid remains or of glauconite or volcanic glass. These data also are included on the accompanying table.

Taxonomy

Taxonomy of foraminifers follows, where possible, that of Jones (1994). *Osangulariella umbonifera* is thus used in place of *Nuttallides umbonifera*. The generic name *Cibicides* is preferred to *Cibicidoides* where relevant. A few species are left in open nomenclature. Unless readily identifiable, species of *Lagena* and *Fissurina* are not differentiated.

RESULTS

Magnetostratigraphy

Results of the magnetostratigraphic determinations (see the "Supplementary Materials" contents list) are shown in Figures F3 and F4. The concentration of dependent magnetic parameters is given in Figure F3. Note that several hiatuses are present but that the Gauss Chron, which is the subject of much discussion, is well defined, although the top of the Gauss is missing as at many sites in the Southern Ocean. Figure F4 shows the concentration of independent magnetic parameters that can be used for mineralogical interpretations. For instance, estimates of the concentration of ferrimagnetic minerals present in our samples can be obtained from some parameters such as k (low-field magnetic susceptibility), IRM, and ARM.

Normalizing these parameters by the susceptibility compensates for variations in concentration and, hence, for example, the k_{ARM} (anhysteretic susceptibility)/k ratio varies inversely with magnetic particle size and is therefore a useful granulometric parameter. The interpretation of this ratio may be complicated by significant amounts of superparamagnetic or paramagnetic phases.

The S-ratio ($S_{-0.3}$) is very useful for discriminating ferrimagnetic grains (such as magnetite) from high-coercivity antiferromagnetic grains such as goethite (α-FeOOH) or hematite (α-Fe_2O_3). So, downcore variations of this parameter may be associated with changing mineralogy. Values close to –1 indicate lower coercivity and a ferrimagnetic mineralogy (e.g., magnetite); values closer to 0 indicate a higher coercivity, possibly an antiferromagnetic (e.g., hematite) mineralogy. Finally, with the magnetic mineralogy constrained as magnetite, the ARM/IRM ratio can be used as a magnetic grain-size indicator too, be-

F3. Concentration-dependent parameters, p. 22.

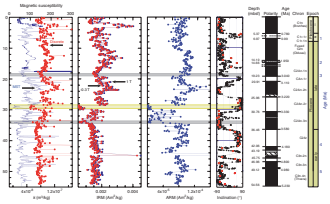

F4. Concentration-independent parameters, p. 23.

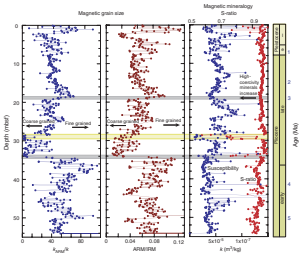

cause the ARM is more effective in activating finer magnetite grains than the IRM.

Figure F5 shows the postcruise revised magnetostratigraphy, based on further laboratory work, and integration with biostratigraphy (marine diatoms and radiolarians). The essential difference from the shipboard interpretation is that the Olduvai is now the "fused" Jaramillo and Olduvai (i.e., Subchrons C1r.1n and C2n are now fused) and the reversed interval between those two subchrons is lost in a hiatus. Because the Pliocene/Pleistocene boundary occurs just above the Olduvai Subchron (Berggren et al., 1995), this boundary must lie in the hiatus (Florindo et al., in press). Additional disconformities must be present near 6.1, 14.3, 15.6, and ~16 mbsf (Florindo et al., in press). (See Fig. F3 caption for data sources).

F5. Magnetostratigraphic record, p. 24.

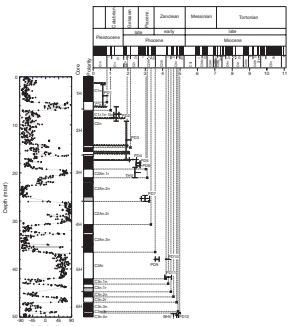

Granulometry

Figure F6 shows the combined results of our granulometric analyses (see the "Supplementary Materials" contents list). Texturally, all samples fall in the mud category as follows: mud, sandy mud, slightly gravelly mud, and slightly gravelly sandy mud. One sample was gravelly mud (after Folk, 1980). The preponderance of mud is indicated by the mud percentage line (only shown for comparison purposes). Sand (area between the gravel and the gravel and sand lines is present in low abundance) (see below). It increases noticeably in the upper 15 m because of the presence of (mainly planktonic) foraminifers in the sand-sized fraction.

F6. Granulometry, p. 25.

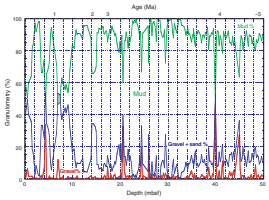

All samples, regardless of textural classification, have a sand-sized component (0.0625–2 mm), but many samples are without a gravel component. Below 15 mbsf, the 0.15- to 2-mm fractions of the sand-sized components consist primarily of lithogenous (terrigenous) material—biogenous components (mainly radiolarians) are rare. Lithogenous components are quartz, feldspar, mafic minerals, lithic fragments of all three rock families, coal, and so on. Quartz consists of several populations, including clear and clouded quartz, quartz with rutile and other inclusions, and quartz as component of lithic fragments.

Although some quartz grains are well rounded and a few have the characteristics of wind-blown grains, the vast majority of quartz grains exhibit the mechanical breakage features such as conchoidal fractures typical of glacial environments, steplike fractures, and so on. No, or very little, rounding is discernible on these grains. The preponderance of quartz grains with "glacial" features suggests that (intermittent) ice rafting occurred throughout the time interval studied here (see Warnke et al., 2001).

A remarkable component of the same sand-size fractions is "garnet-colored" garnet. It is optically indistinguishable from garnet recently discovered in Pleistocene samples in piston core TN0-57-6-PC4, raised in the South Atlantic (42°52.1′S, 8°57.7′E; 3751 m), suggesting that icebergs calving from marine termini in Prydz Bay may occasionally reach that far-distant site (Teitler et al., 2002). Garnet grains show mechanical breakage features indicative of glacial environments.

Diffuse Reflectance Spectrophotometry (DRS)

Sediment Brightness Determined from Spectral Data

Sediment brightness (sometimes termed lightness) is calculated as the area under a spectral curve in the visible (400–700 nm) portion of the spectrum. Brightness measured in marine sediments commonly shows a positive correlation with calcium carbonate, especially in pelagic sediments, and thus is sometimes used as a proxy for carbonate content; however, other factors can also influence brightness (see Balsam et al., 1999, for detailed discussion about interpreting brightness as a function of carbonate content). Figures F2 and F7 show the brightness for the HiRISC section (0–54 mbsf) in Hole 1165B. Figure F8 shows percent reflectance curves for six color bands. Note that in the upper 10 m of the section the brightness seems to correlate with the carbonate content (Fig. F2). However, for the remainder of the section where carbonate is essentially zero, the brightness also varies widely and thus must be related to mineralogical components other than carbonate. For example, the brightness curve seems to correlate quite well with grain-size magnetic parameters, bulk density, and natural gamma radiation curves from the HiRISC section (Figs. F3, F4, F5). In particular, a major change in sediment properties at the beginning of the late Pliocene in these parameters is clearly recorded by an overall sharp decrease in brightness just above 34 mbsf (Figs. F2, F7).

The brightness for the HiRISC section derived from shipboard measurements using the Minolta CM-2002 spectrophotometer is also shown in Figure F7. During Leg 188, the Minolta instrument was mounted on the archive multisensor track (see O'Brien, Cooper, Richter, et al., 2001, for details) and all spectral measurements were automated and performed on the archive half of each core. Because of this automated process, erroneous measurements were commonly made at gaps, voids, missing intervals of core, and so on. The Minolta data shown in Figure F7 are an edited subset of the original shipboard data set from which these erroneous measurements have been deleted as far as possible (see Damuth and Balsam, this volume). Note that the shipboard brightness data fluctuations correlate quite well with the Perkin-Elmer-derived data, except that the brightness for the sediments measured with the Minolta is consistently lower than those values measured with the PerkinElmer. We have conducted several studies on cores from previous ODP legs comparing shipboard Minolta measurements, which by necessity must be conducted on wet cores, with PerkinElmer measurements, which must be made on dried, ground core sediments (Balsam et al., 1997, 1998, 1999; Balsam and Damuth, 2000). These studies showed that water in the sediments mutes the brightness. However, when both sets of reflectance curves are processed using a first-derivative transformation, the shipboard and shore-based analyses are quite similar and suggest that accurate, reliable spectral data can be obtained from wet cores at sea using the Minolta spectrophotometer.

Interpretation of Sediment Components and Minerals with DRS Using Factor Analysis

Interpretation of sediment components and minerals was carried out by factor analysis of the first-derivative values calculated at 10-nm intervals from the percent reflectance values. Details of the methodology, including background and advantages of VIS spectral analysis are pro-

F7. Changes in brightness, p. 26.

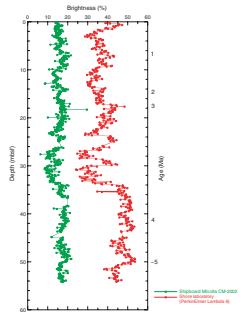

F8. Percent reflectance for six color bands, p. 27.

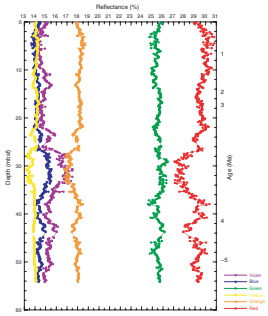

vided in **Damuth and Balsam** (this volume), Balsam and Deaton (1991), Balsam et al. (1997), and Balsam and Damuth (2000). **Damuth and Balsam** (this volume) identified five factors from the sediments at Site 1165, and we interpret these factors as follows:

Factor 1: goethite and ripidolite, a chlorite mineral;
Factor 2: organic matter;
Factor 3: a combination of clay minerals, probably montmorillonite;
Factor 4: maghemite; and
Factor 5: hematite.

See **Damuth and Balsam** (this volume) for detailed explanation of these factor interpretations.

Factor interpretation can be aided by plotting the downhole distribution of each factor using factor scores, which indicate how important each factor is in each sample (e.g., Figs. **F9, F10, F11, F12, F13**). These downhole factor scores presumably show how the various minerals represented by each factor vary downhole. Ideally, these downhole plots are then compared to downhole distributions of various sediment components identified by other means (e.g., X-ray diffraction). There are some important similarities and differences between reflectance data and data generated by other commonly used analytical techniques such as XRD. In several ways, reflectance data derived from DRS are similar to XRD. First-derivative peak height, like the height of X-ray peaks, is a function of both the concentration of a substance (mineral for XRD) and the composition of the matrix in which it is found (Deaton and Balsam, 1991; Balsam et al., 1999). DRS data differ from XRD data in three important respects. First, DRS is not limited to crystalline material; spectra can be obtained from any substance. Second, the heights of first-derivative peaks are not only a function of mineral concentration and matrix material but also are a function of the "spectral strength" of a substance. Some substances (e.g. hematite) have a persistent spectral signal that is capable of concealing the peaks of other substances. Third, for some substances, the limits of resolution of DRS differ significantly from those of XRD. For example, depending on the matrix, hematite can be detected at a concentration of ~0.01% by weight with DRS, whereas with XRD, the limit of resolution without special sample preparation is ~1% (Deaton and Balsam, 1991). To date, limits of resolution with DRS have been determined for only a very few minerals, sediment components, and combinations of components. For XRD, a similar statement applies for many minerals and mineral combinations.

In the HiRISC section of Hole 1165B (0–54 mbsf), factors 1 and 2 exhibit high scores through most of the section, with the exception of a low in both factors centered at ~30 m (Figs. **F9, F10**). Factors 3 and 4 exhibit high values primarily below 30 m (Figs. **F11, F12**). Factor 5 exhibits higher-frequency variation than the other factors and, with the exception of a few points, contains primarily high values below ~10 m (Fig. **F13**). Despite apparent similarities in their downhole patterns, few of the factors are highly correlated to each other. The highest linear correlation is exhibited by factors 2 (organic matter) and 5 (hematite), which has $r^2 = 0.51$. This correlation is difficult to explain. The next highest linear correlation is factors 3 (montmorillonite and illite) and 4 (maghemite), which has $r^2 = 0.36$. One possible explanation for this correlation is that the maghemite is being transported with clay minerals or is produced by the erosion of clays. Factor 1 (goethite and ripidolite) and factor 5 (hematite) exhibit a linear correlation with $r^2 = 0.23$. Al-

F9. Factor scores for factor 1 (goethite and ripidolite), p. 28.

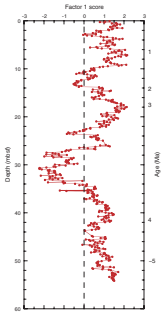

F10. Factor scores for factor 2 (organic matter), p. 29.

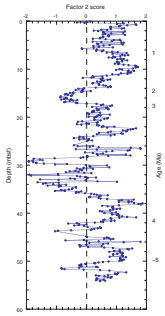

F11. Factor scores for factor 3 (montmorillonite and illite), p. 30.

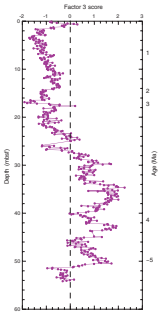

F12. Factor scores for factor 4 (maghemite), p. 31.

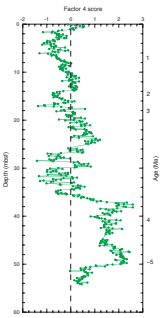

though hematite and goethite may form at high temperatures by thermal oxidation (Dunlop and Özdemir, 1997), they may also form at low temperatures by oxidation in soils and during chemical weathering. Under surficial conditions and especially in soils, hematite and goethite are end-members of oxidizing chemical processes, with hematite forming under dry and hot conditions and goethite under more humid conditions (Maher, 1998; Maher and Thompson, 1999). There is substantial overlap in their formation and both are commonly found together. Also formed by chemical processes taking place in soils and in rock rubble are a variety of clay minerals. The fact that this factor analysis separates hematite and goethite into two factors suggests that these minerals have different sources. Factor 3 (montmorillonite and illite) and factor 5 (hematite) exhibit a linear correlation with $r^2 = 0.21$. As above, one possible explanation of this correlation is that the hematite is being transported with clay minerals or is produced by the erosion of clays. No other factors exhibit linear correlations with $r^2 > 0.2$.

F13. Factor scores for factor 5 (hematite), p. 32.

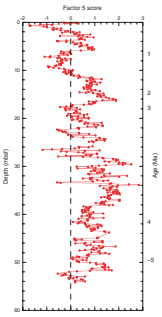

Stable Isotopes

N. pachyderma (s.) $\delta^{18}O$ values range from 3.89‰ to 4.96‰ (see Fig. **F14**) and generally increase during the late Pliocene–Pleistocene, reflecting the transition to cooler temperatures and globally increased ice volume (see the **"Supplementary Materials"** contents list). There appears to be several glacial–interglacial cycles recorded in this section. Between the base and what was assumed to be the top of the Olduvai Subchron (1.95–1.77 Ma; 14.10–6.97 mbsf) during the leg, four glacial–interglacial cycles are recorded (note, however, that the top of the Olduvai is missing—see above). Based on the location of an unconformity (at ~6 mbsf) below the Brunhes/Matuyama paleomagnetic reversal (0.78 Ma; 5.37 mbsf), much of the early Pleistocene is missing. The glacial–interglacial cycle recorded above needs further investigation. An unconformity occurs at ~3 mbsf, based on the jump in values, and further age control will be necessary to identify the glacial–interglacial periods above this point.

F14. Stable isotopes, p. 33.

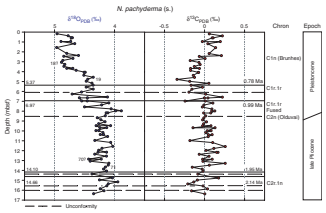

N. pachyderma (s.) $\delta^{13}C$ values range from –0.344‰ to 0.259‰ and fluctuate in accordance with $\delta^{18}O$ changes. During the inferred interglacial periods $\delta^{13}C$ values are generally higher, indicating an increase in primary production that leaves surface waters enriched in ^{13}C due to the preferential uptake of ^{12}C. The small amplitude of glacial–interglacial $\delta^{13}C$ changes (0.4‰) suggests that changes in surface water primary production were relatively small in the region during the late Pliocene–Pleistocene.

Clays

Results of the clay mineral analyses (see the **"Supplementary Materials"** contents list) are shown in Figure **F15.** All results are plotted against depth. The clay mineral assemblages are dominated by smectite, illite, and kaolinite. The smectite concentration is variable, with values mainly between 0% and 30%. Illite fluctuates less; concentrations are mainly 50%–80%, and kaolinite varies mainly between 10% and 20%. Chlorite concentrations are mainly 0%–10%.

F15. Clay mineral distribution, p. 34.

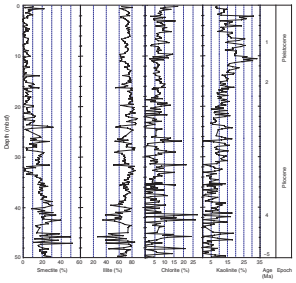

Cyclicity of Clay Mineral Assemblages during the Late Quaternary

Late Quaternary variations of clay mineral assemblages deposited on the continental rise off Prydz Bay show possible cyclicity with higher smectite concentrations during prominent interglacials. We presume that the cyclicity in clay mineral assemblages observable in Prydz Bay is the same type that was observed in the area of the Antarctic Peninsula (Hillenbrand, 2000). Smectite decreases and chlorite increases from 50 to 0 mbsf. Chlorite concentrations mirror slightly the smectite variations.

In general, during interglacial periods smectite is delivered by bottom-current transport along the continental rise. The decrease of smectite during glacial periods may be a consequence of climate-induced changes in depositional processes on the margin (see Pudsey and Camerlenghi, 1998; Rebesco et al., 1998; Hillenbrand, 2000; Pudsey, 2000; see also Grobe and Mackensen, 1992).

Pliocene to Quaternary Clay Mineral Assemblages in Sediments at Site 1165

According to the existing age model, the stratigraphic sequence of Site 1165 (uppermost 50 mbsf) extends back to ~5.0 Ma. Throughout this interval, the clay mineral content is characterized by major fluctuations of individual clay minerals, particularly smectite and chlorite. Short-term cyclic changes in clay mineral assemblages deposited at Site 1165 occur throughout the Pliocene and Quaternary independent of changes in the clay content. We note that changes in clay mineral composition are also reflected in the other proxies, described earlier. For instance, the noticeable change detected both by rock magnetic investigations and spectrographic methods at ~34 mbsf is clearly indicated in the composition of the clay mineral suite. At this level, smectite decreases whereas kaolinite increases. Illite and chlorite also show variability. In particular, there is a slight but persistent increase in chlorite.

Foraminifer Analyses

The section studied lies in the latest Pliocene–Pleistocene, but a large section (1.70–9.25 mbsf) has not been zoned. Foraminifer faunas are very highly dominated by *Neogloboquadrina pachyderma* (Ehrenberg), commonly to ≥99.5%, suggesting that benthic productivity was generally low. This is consistent with the very low content of infaunal species. Planktonic percentages significantly less than 99.5% are due to preferential dissolution of planktonic specimens. Many residues consist very dominantly of *N. pachyderma* with little other content.

The section can be divided into the following intervals on the basis of variation in planktonic percentage, absolute counts of specimens, and features of the benthic fauna (Table T1):

1. Surface–0.95 mbsf: characterized by high planktonic numbers and high planktonic percentages, with modest exceptions at 0.57 and 0.95 mbsf. Residues are dominated by biogenic material, but this varies between foraminifers and radiolarians. This section lies within the *Thalassiosira lentiginosa* Zone, which is younger than 0.66 Ma (Shipboard Scientific Party, 2001).

2. 1.17–6.27 mbsf: characterized by low planktonic numbers and generally high planktonic percentages, with modest exceptions at 1.37, 1.97, 3.87, 4.07, and 4.77 mbsf, where planktonic numbers are higher. Residues are dominated by terrigenous sediment. Very few contain manganese oxides, but this accessory increases toward the base of the interval. To 1.70 mbsf, this section is attributed to the *T. lentiginosa* Zone. There is a hiatus at ~6 mbsf, but the section remains unzoned paleontologically.
3. 6.47–11.76 mbsf: characterized by high planktonic numbers and generally high planktonic percentages with exceptions at 8.87 and 9.97 mbsf and a general decline in planktonic numbers below 11.96 mbsf. Samples are dominated by *N. pachyderma,* and radiolarians are virtually absent from the samples. Benthic foraminifers are more abundant and diverse than in the sections above and below. It is the only section in which *Cibicides* is a significant component. The section to 9.25 mbsf remains unzoned paleontologically. Below that depth, it has been assigned to the *Fragilariopsis kerguelensis* Zone of the late Pliocene–early Pleistocene. *Globorotalia puncticulata*, indicating some "warmth," occurs at 7.50 mbsf within this section.
4. 11.76 mbsf–base: characterized by low planktonic numbers and generally reduced planktonic percentages, but the figures are somewhat erratic toward the barren part of the section deeper than 15 mbsf. There is a transition interval at 11.57–13.27 mbsf in which dominance by terrigenous sediment or *N. pachyderma* varies from sample to sample. *Osangulariella umbonifera* and *Alabaminoides exiguus* are the only constant benthic foraminifer components. Radiolarians are more important than in the interval above but still generally are present in trace amounts. Manganese oxides become more important components of residues through this interval. This section also has been assigned to the *F. kerguelensis* Zone.

Intervals 2 and 4 are strongly influenced by carbonate dissolution and represent times of greater impact of undersaturated seawater.

Throughout the section, the benthic fauna is dominated by the same species, namely, *A. exiguus, O. umbonifera, Melonis pompilioides*, and *Fissurina* spp. *Pullenia* spp. and agglutinated species are noteworthy at some intervals. Other species are less consistent in their occurrence. Infaunal species are rare throughout, suggesting that nutrient flux to the seafloor was limited.

Depth Migration of Benthic Species?

The constant appearance together of *O. umbonifera, M. pompilioides,* and *A. exiguus* is very strong evidence that the benthic fauna is in situ and that there has been no transport of benthic species from shallower depths to the site of deposition. These species together are taken by van Morkhoven et al. (1986) as markers of abyssal environments deeper than 2000 m. Many other benthic species recorded here have depth ranges shallower than 2000 m as their shallower limit, and they are to be expected in abyssal faunas.

Carbonate Compensation Depth Influences

The site was drilled in 3537 m water depth, ~270 km north of the continental shelf edge, taken as being the 500-m isobath. The carbonate compensation depth (CCD) in upper continental slope depths is at ~1500 m (Quilty, 1985; Poisson et al., 1987), and thus the site of Site 1165 is expected, at first sight, to be well below the current CCD. This assumption may be incorrect because of the complexities of local oceanography, including the formation of some Antarctic Bottom Water in Prydz Bay and its northwesterly flow, possibly over the drill site (Shipboard Scientific Party, 2001).

It seems clear that the major influence on preservation or destruction of the carbonate fossils is variation in the depth of the CCD, possibly modified by the time of exposure of the seafloor to undersaturated water.

Sedimentation Rate Variation and Hiatuses

A hiatus was recorded at ~6 mbsf by the Shipboard Scientific Party (2001), and the possibility of other short hiatuses was mentioned (see also above). None are significant enough to have any obvious impact on the sedimentation rate curve at the scale produced by Shipboard Scientific Party (2001), but there must be some impact at a greater level of differentiation.

PRELIMINARY CONCLUSIONS

Although detailed interpretations of the combined data sets must await further work, a few conclusions can be presented at this time. In the whole debate about Antarctic cryospheric evolution during the Pliocene, some authors have classified all authors as belonging to one of two categories: "dynamicists" and "stabilists." Such labels should be abandoned because if we ask, "Who is right, the stabilists or the dynamicists?" The answer must be "both" (see also Quilty, 1996): there is no doubt about the antiquity of landscape features and glacial ice in the mountains near the Dry Valleys as proposed (e.g., Marchant and Lewis, 2002), based on 75 laser-fusion age dates of ash fall deposits and numerous cosmogenic-nuclide analyses of boulders. At the same time, the interpretation of seismic lines and stable isotopic records (e.g., Hart, 2001) suggests that the margin of the ice sheet has advanced and retreated across the continental margin several times during the Pliocene, suggesting a dynamic behavior, at least of the ice sheet margin. In addition, field work in the Vestfold Hills (Soersdal Formation) suggests that during parts of the early Pliocene the ice sheet grounding line was far landward of its present location (Whitehead et al., 2001). However, vertical movements of the coastal area need to be better constrained for an evaluation of absolute grounding-line movements.

Our analyses likewise suggest a dynamic behavior of the ice sheet margin, reflected by the somewhat surprising fluctuations in all measured parameters, particularly magnetic parameters, brightness and color, stable isotopes, and clays and clay mineral composition. For instance, at 34 mbsf, brightness, ARM, k, and ARM/IRM all change. Smectite percent decreases upsection while kaolinite percent increases. Most investigators agree that these changes reflect changes in the specific location of the source area within the Lambert Graben drainage area. This

conclusion is in agreement with similar conclusions drawn by the Shipboard Scientific Party (2001) for the older Miocene portion of Site 1165. The remarkable change at 34 mbsf occurred in the lowermost normal interval of the Gauss Chron, at ~3.4–3.5 Ma(?). A correlation with nearby drill sites of ODP Legs 119 and 120 is not immediately obvious, perhaps because the review of the results of these sites (Ehrmann et al., 1992) essentially dealt with the "big picture" of Antarctic climate evolution. In addition, there are sites on the Kerguelen Plateau that yielded a record of ice rafting for the last 10 m.y. (Ehrmann et al., 1992). The combined Sites 745/74 show a strong influx of ice-rafted debris at 4.5–4.3 Ma. Site 751 shows an increase in ice rafting at 3.2–2.9 Ma. None of these records can be confidently correlated with ours.

Going farther afield, we speculate that the "big change" at Site 1165 at 34 mbsf may be coeval with the beginning of ice rafting at Leg 114 Site 704 in the South Atlantic. This beginning occurred during marine isotope Stage (MIS) MG2 and suggests a drop in sea-surface temperature at that location (i.e., a northward movement of the polar frontal systems).

In the HiRISC interval at Site 1165, starting from the bottom, smectite percent decreases upsection to ~34 mbsf. Above a transitional interval from ~34 to ~22 mbsf the clay mineralogy is characterized by a smectite-poor assemblage. Illite concentrations do not seem constant but fluctuate in concert (antiparallel) with smectite. At this stage, we have no straightforward explanation for these changes. A possible explanation is that there were temporal variations in supply from the source rocks (for example, by progressive erosion through successive units in the source area or by switching of source regions). A second explanation is that these changes possibly reflect a climatic modulation of weathering type and transport mechanism of these sediments. The clay mineral assemblage and the likely presence of maghemite below ~35 mbsf (factor 4) may be due to enhanced pedogenesis associated with a relatively warmer and wetter climate. If our "weathering hypothesis" is correct, then this observation further supports the hypothesis that the change at 34 mbsf may coincide with the beginning of ice rafting observed at Site 704 in the South Atlantic during MIS MG2. Details, causes, and correlations of these changes must still be worked out.

Another important result of detailed, integrated magnetostratigraphic and biostratigraphic work is the identification of significant hiatuses (i.e., 100 k.y. or more) within the HiRISC interval, suggesting occasional strong erosional events on the continental rise. Similar conclusions were recently drawn by Escutia et al. (2003) for the continental rise area off Wilkes Land, East Antarctica.

Our cooperative research will hopefully continue. Some of the changes indicated in the integrated data set for the East Antarctic Ice Sheet need to be better constrained, characterized, and correlated with events on the Antarctic Peninsula (West Antarctic Ice Sheet) and elsewhere.

ACKNOWLEDGMENTS

This research used samples and data provided by the Ocean Drilling Program (ODP). The ODP is sponsored by the U.S. National Science Foundation (NSF) and participating countries under management of Joint Oceanographic Institutions (JOI), Inc. Funding for this research was provided JOI-USSAC (United States Science Advisory Committee),

and participating national funding agencies. We thank John Barron and Alan Cooper for constructive reviews; however, all errors of commission or omission are our own.

REFERENCES

Allen, C.P., and Warnke, D.A., 1991. History of ice rafting at Leg 114 sites, subantarctic/South Atlantic. *In* Ciesielski, P.F., Kristoffersen, Y., et al., *Proc. ODP, Sci. Results,* 114: College Station, TX (Ocean Drilling Program), 599–607.

Balsam, W.L., and Damuth, J.E., 2000. Further investigations of shipboard vs. shore-based spectral data: implications for interpreting Leg 164 sediment composition. *In* Paull, C.K., Matsumoto, R., Wallace, P., and Dillon, W.P. (Eds.), *Proc. ODP, Sci. Results,* 164: College Station, TX (Ocean Drilling Program), 313–324.

Balsam, W.L., Damuth, J.E., and Schneider, R.R., 1997. Comparison of shipboard vs. shore-based spectral data from Amazon-Fan cores: implications for interpreting sediment composition. *In* Flood, R.D., Piper, D.J.W., Klaus, A., and Peterson, L.C. (Eds.), *Proc. ODP, Sci. Results,* 155: College Station, TX (Ocean Drilling Program), 193–215.

Balsam, W.L., and Deaton, B.C., 1991. Sediment dispersal in the Atlantic Ocean: evaluation by visible light spectra. *Rev. Aquat. Sci.,* 4:411–447.

Balsam, W.L., Deaton, B.C., and Damuth, J.E., 1998. The effects of water content on diffuse reflectance measurements of deep-sea core samples: an example from ODP Leg 164 sediments. *Mar. Geol.,* 149:177–189.

————, 1999. Evaluating optical lightness as a proxy for carbonate content in marine sediment cores. *Mar. Geol.,* 161:141–153.

Bart, P.J., 2001. Did the Antarctic ice sheets expand during the early Pliocene? *Geology,* 29:67–70.

Bé, A.W.H., 1977. An ecological, zoogeographic and taxonomic review of recent planktonic foraminifera. *In* Ramsey, A.T.S. (Ed.), *Oceanic Micropaleontol.,* 19:150–192.

Berggren, F.C., Kent, D.V., Swisher, C.C., and Aubry, M.P., 1995. *A Revised Cenozoic Geochronology and Chronostratigraphy.* Spec Publ.—SEPM (Soc. Sediment. Geol.), 54:129–212.

Biscaye, P.E., 1964. Distinction between kaolinite and chlorite in recent sediments by X-ray diffraction. *Am. Miner.,* 49:1281–1289.

Burckle, L.H., Mortlock, R., and Rudolph, S., 1996. No evidence for extreme, long term warming in early Pliocene sediments of the Southern Ocean. *Mar. Micropaleontol., 27*:215–226.

Charles, C.D., and Fairbanks, R.G., 1990. Glacial to interglacial changes in the isotopic gradients of Southern Ocean surface water. *In* Bleil, U., and Thiede, J. (Eds.), *Geological History of Polar Oceans: Arctic Versus Antarctic:* Dordrecht, The Netherlands (Kluwer Academic), 519–538.

Deaton, B.C., and Balsam, W.L., 1991. Visible spectroscopy—a rapid method for determining hematite and goethite concentration in geological materials. *J. Sediment. Petrol.,* 61:628–632.

Dowsett, H.J., Barron, J.A., Poore, R.Z., Thompson, R.S., Cronin, T.M., Ishman, S.E., and Willard, D., 1999. Middle Pliocene paleoenvironmental reconstruction: PRISM2. *Open-File Rep.—U.S. Geol. Surv.,* 99-535:558.

Dunlop, D.J., and Özdemir, Ö., 1997. *Rock Magnetism: Fundamentals and Frontiers:* Cambridge (Cambridge Univ. Press).

Ehrmann, W.U., Hambrey, M.J., Baldauf, J.G., Barron, J., Larsen, B., Mackensen, A., Wise, S.W., and Zachos, J.C., 1992. History of Antarctic glaciation: an Indian Ocean perspective. *In* Duncan, R.A., Rea, D.K., Kidd, R.B., von Rad, U., and Weissel, J.K. (Eds.), *Synthesis of Results from Scientific Drilling in the Indian Ocean.* Geophys. Monogr., 70:423-446.

Escutia, C., Warnke, D., Acton, G.D., Barcena, A., Burckle, L., Canals, M., and Frazee, S., 2003. Sediment distribution and sedimentary processes across the Antarctic Wilkes Land margin during the Quaternary. *Deep-Sea Res., Part II.,* 50:1481–1508.

Florindo, F., Bohaty, S.M., Erwin, P.S., Richter, C., Roberts, A.P., Whalen, P.A., and Whitehead, J.M., in press. Magnetobiostratigraphic chronology and palaeoenvironmental history of Cenozoic sequences from ODP Sites 1165 and 1166, Prydz Bay, Antarctica. *In* Florindo, F., Cooper, A.K., and O'Brien, P.A. (Eds.), *Antarctic Cenozoic Paleoenvironments: Geologic Record and Models*. Palaeogeogr., Palaeoclimatol., Palaeoecol.

Folk, R.L., 1980. *Petrology of Sedimentary Rocks* (2nd ed.): Austin, TX (Hemphill's).

Grobe, H., and Mackensen, A., 1992. Late Quaternary climatic cycles as recorded in sediments from the Antarctic continental margin. *In* Kennett, J.P., and Warnke, D.A. (Eds.), *The Antarctic Paleoenvironment: A Perspective on Global Change* (Pt. 1). Antarct. Res. Ser., 56:349–376.

Hambrey, M.J., and Barrett, P.J., 1993. Cenozoic sedimentary and climatic record, Ross Sea region, Antarctica. *In* Kennett, J.P., and Warnke, D.A. (Eds.), *The Antarctic Paleoenvironment: A Perspective on Global Change* (Pt. 2). Antarct. Res. Ser., 60:91–124.

Hardy, R., and Tucker, M., 1988. X-ray powder diffraction of sediments. *In* Tucker, M. (Ed.), *Techniques in Sedimentology:* Oxford (Blackwell Scientific Publications), 191–228.

Hillenbrand, C.-D., 2000. *Glaciomarine Sedimentation on the Continental Margins of the Amundsen and Belllingshausen Seas, West Antarctica: Indications for Paleoenvironmental Changes during the Quaternary Climatic Cycles:* Bremerhaven (Alfred Wegener Institute for Polar and Marine Research).

Hodell, D.A., 1993. Late Pleistocene paleoceanography of the South Atlantic sector of the Southern Ocean: Ocean Drilling Program Hole 704A. *Paleoceanography,* 8:47–67.

Hodell, D.A., and Warnke, D.A., 1991. Climatic evolution of the Southern Ocean during the Pliocene epoch from 4.8 to 2.6 million years ago. *Quat. Sci. Rev.,* 10:205–214.

Hrouda, F., 1994. A technique for the measurement of thermal changes of magnetic susceptibility of weakly magnetic rocks by the CS-2 apparatus and KLY-2 Kappabridge. *Geophys. J. Int.,* 118:604–612.

Jones, G.A., and Kaiteris, P., 1983. A vacuum-gasometric technique for rapid and precise analysis of calcium carbonate in sediments and soils. *J. Sediment. Petrol.,* 53:655–660.

Jones, R.W., 1994. *The Challenger Foraminifera:* New York (Oxford).

Kennett, J.P., and Hodell, D.A., 1993. Evidence for relative climate stability of Antarctica during the early Pliocene: a marine perspective. *Geogr. Ann.,* 75A:205–220.

Kirschvink, J.L., 1980. The least-squares line and plane and the analysis of palaeomagnetic data. *Geophys. J. R. Astron. Soc.,* 62:699–718.

Lowrie, W., 1990. Identification of ferromagnetic minerals in a rock by coercivity and unblocking temperature properties. *Geophys. Res. Lett.,* 17:159–162.

Mackensen, A., Grobe, H., Hubberten, H.W., Spiess, V., and Fütterer, D.K., 1989. Stable isotope stratigraphy from the Antarctic continental margin during the last one million years. *Mar. Geol.,* 87:315–321.

Maher, B.A., 1998. Magnetic properties of modern soils and Quaternary loessic paleosols: paleoclimatic implications. *Palaeogeogr., Palaeoclimatol., Palaeoecol.,* 137:25–54.

Maher, B.A., and Thompson, R., 1999. Paleomonsoons I: the magnetic record of paleoclimate in the terrestrial loess and paleosol sequences. *In* Maher, B.A., and Thompson, R. (Eds.), *Quaternary Climates, Environments and Magnetism:* Cambridge (Cambridge Univ. Press), 81–125.

Marchant, D.R., and Lewis, A.R., 2002. Paralyzed landscapes of southern Victoria Land: climate and ice sheet stability since the middle Miocene. *Geol. Soc. Am. Bull.,* 73:4. (Abstract)

Murphy, L., Warnke, D.A., Andersson, C., Channell, J., and Stoner, J., 2002. History of ice rafting at South Atlantic ODP Site 177-1092 during the Gauss and the late Gilbert Chron. *Palaeogeogr., Palaeoclimatol., Palaeoecol.,* 182:183–196.

O'Brien, P.E., Cooper, A.K., Richter, C., et al., 2001. *Proc. ODP, Init. Repts.*, 188 [CD-ROM]. Available from: Ocean Drilling Program, Texas A&M University, College Station TX 77845-9547, USA.

Petschick, R., 2001. MacDiff 4.1.1 Manual. *MacDiff* [Online]. Available from World Wide Web: <http://www.geologie.uni-frankfurt.de/Staff/Homepages/Petschick/RainerE.html>. Revised [2001-05-17]

Poisson, A., Schauer, B., and Brunet, C., 1987. Les rapports des campagnes à la mer: MD53. Indigo 3 à bord du *Marion Dufresne. Publ. Terres Aust. Antarct. Fr.,* 87:77–85.

Pudsey, C.J., 2000. Sedimentation on the continental rise west of the Antarctic Peninsula over the last three glacial cycles. *Mar. Geol.,* 167:313–338.

Pudsey, C.J., and Camerlenghi, A., 1998. Glacial–interglacial deposition on a sediment drift on the Pacific margin of the Antarctic Peninsula. *Antarct. Sci.,* 10:286–308.

Quilty, P.G., 1985. Distribution of foraminiferids in sediments of Prydz Bay, Antarctica. *Spec. Publ.—S. Aust. Dep. Mines Energy,* 5:329–340.

————, 1993. Coastal Neogene sections and their contribution to the ice sheet evolution debate. *In* Kennett, J.P., and Warnke, D.A. (Eds.), *The Antarctic Paleoenvironment: A Perspective on Global Change* (Pt. 2), Antarct. Res. Ser., 60:251–264.

————, 1996. The Pliocene environment of Antarctica. *Pap. Proc. R. Soc. Tasmania,* 130:1–8.

Rebesco, M., Camerlenghi, A., and Zanolla, C., 1998. Bathymetry and morphogenesis of the continental margin west of the Antarctic Peninsula. *Terra Antart.,* 5:715–728.

Robin, G. de Q., 1988. The Antarctic ice sheet, its history and response to sea level and climatic changes over the past 100 million years. *Palaeogeogr., Palaeoclimatol., Palaeoecol.,* 67:31–50.

Shipboard Scientific Party, 2001. Leg 188 summary: Prydz Bay–Cooperation Sea, Antarctica. *In* O'Brien, P.E., Cooper, A.K., Richter, C., et al., *Proc. ODP, Init. Repts.,* 188: College Station TX (Ocean Drilling Program), 1–65.

Teitler, L.F., Warnke, D.A., Venz, K.A., and Hodell, D.A., 2002. The record of garnets and *Dyctiocorine (profunda?)* at Sites TN057-6-PC4 and ODP 177-1090 (Agulhas Ridge, South Atlantic). *Geol. Soc. Am. Bull.,* 104:144. (Abstract)

van Morkhoven, F.P.C.M., Berggren, W.A., and Edwards, A.S., 1986. *Cenozoic Cosmopolitan Deep-Water Benthic Foraminifera.* Bull. Cent. Rech. Explor.—Prod. Elf-Aquitaine, Mem. 11.

Warnke, D.A., Marzo, B., and Hodell, D.A., 1996. Major deglaciation of East Antarctica during the early late Pliocene? Not likely from a marine perspective. *In* Poore, R.Z., and Sloan, L.C. (Eds.), *Climates and Climate Variability of the Pliocene.* Mar. Micropaleontol., 27:237–251.

Warnke, D.A., and ODP Leg 188 Shipboard Scientific Party, 2001. Pliocene coarse-grained debris at Ocean Drilling Program Site 188-1165, Prydz Bay, Antarctica. *In* Florindo, F., and Cooper, A. (Eds.), *The Geologic Record of the Antarctic Ice Sheet from Coring, Drilling, and Seismic Studies.* Quad. Geofis., 16:191–192.

Webb, P.-N., and Harwood, D.M., 1991. Late Cenozoic glacial history of the Ross Embayment, Antarctica. *Quat. Sci. Rev.,* 10:215–223.

Whitehead, J.M., Quilty, P.G., Harwood, D.M., and McMinn, A., 2001. Early Pliocene paleoenvironment of the Sørsdal Formation, Vestfold Hills, based on diatom data. *Mar. Micropaleontol.,* 41:125–152.

Figure F1. Location map.

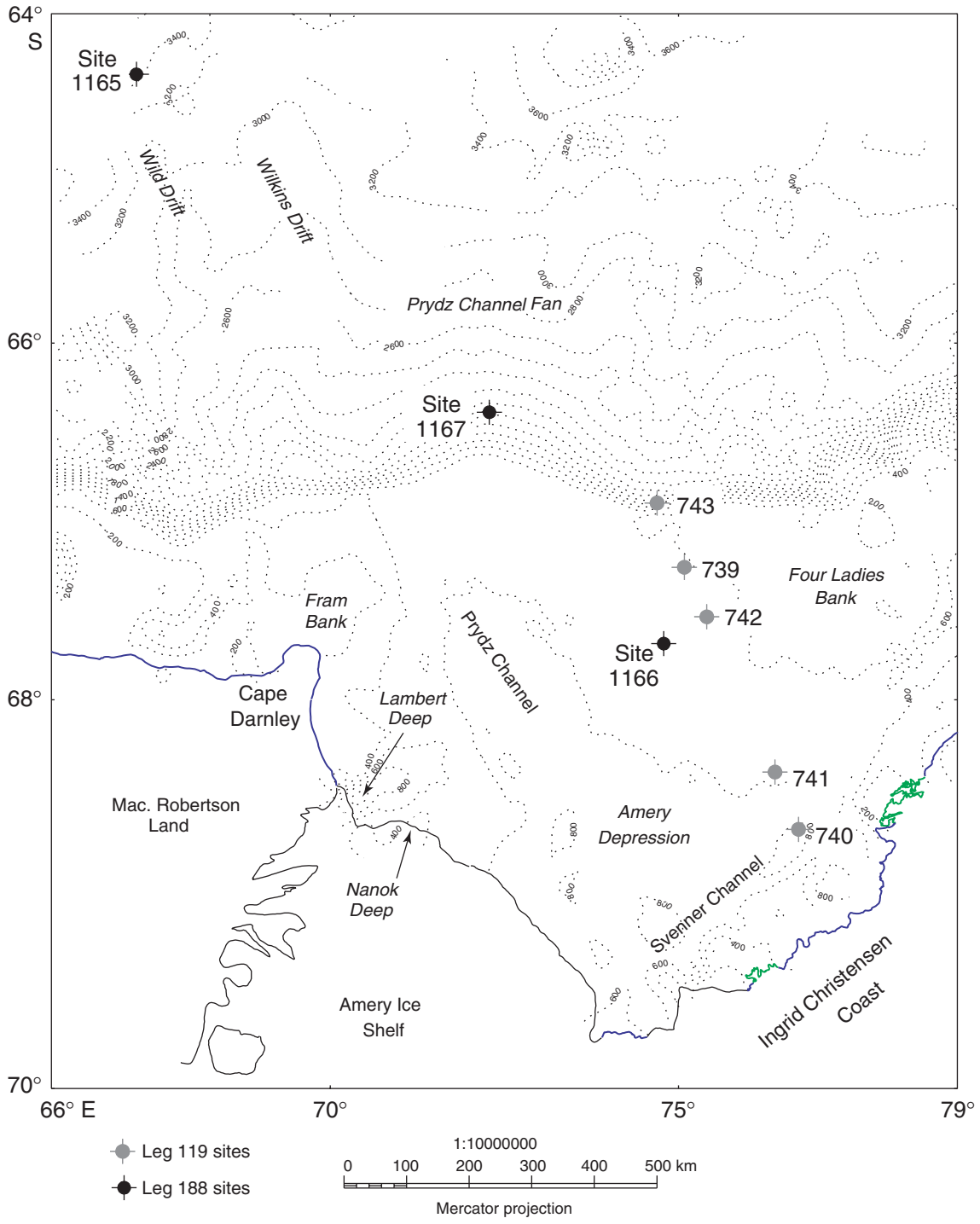

Figure F2. Calcium carbonate content and brightness curves for the HiRISC section of Hole 1165B (see **Damuth and Balsam,** this volume, their table **T1,** for sample locations and values).

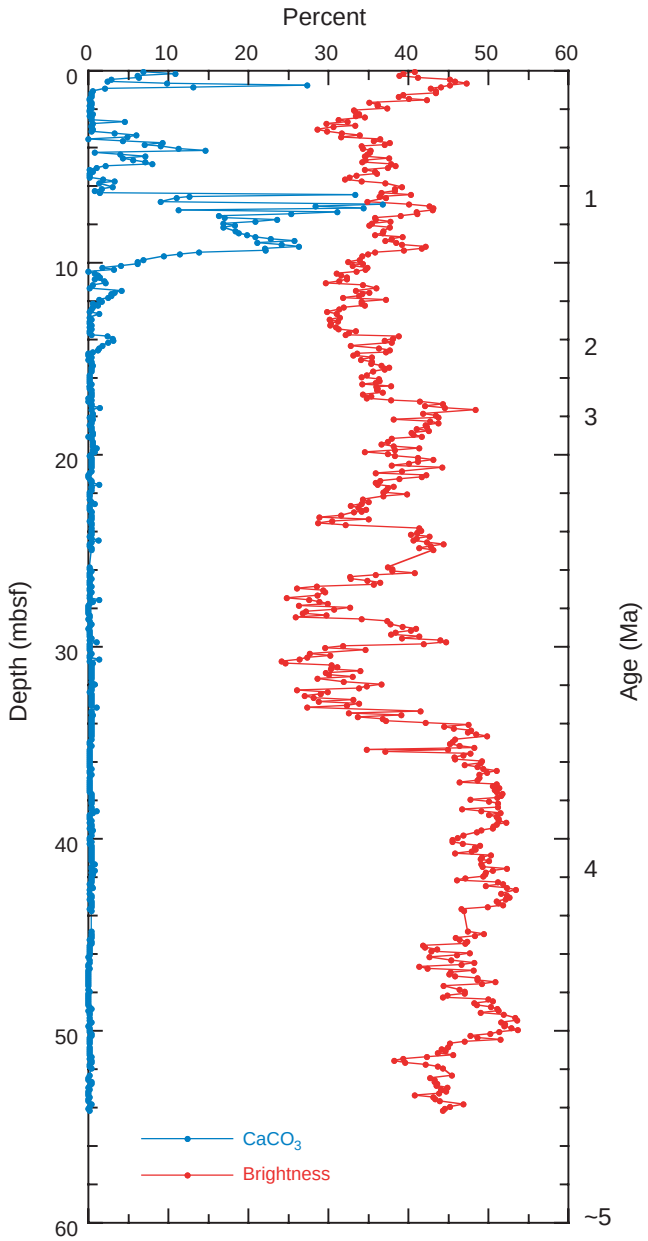

Figure F3. Concentration-dependent parameters as a function of stratigraphic depth for the uppermost 54 m at Site 1165. **A.** Low-field magnetic susceptibility (*k*) from discrete samples and from whole cores. **B.** Isothermal remanent magnetization (IRM) imparted in a direct-current (DC) field of 1 T compared to the IRM imparted in a field of 0.3 T. **C.** Anhysteretic remanent magnetization (ARM) imparted with a 100-mT AF and 0.05-mT DC bias field. **D–F.** Magnetostratigraphy and age model are shown to the right. Chron ages for polarity reversal boundaries are from Berggren et al. (1995). MST = multisensor track. (See the **"Supplementary Materials"** contents list for magnetostratigraphic data.)

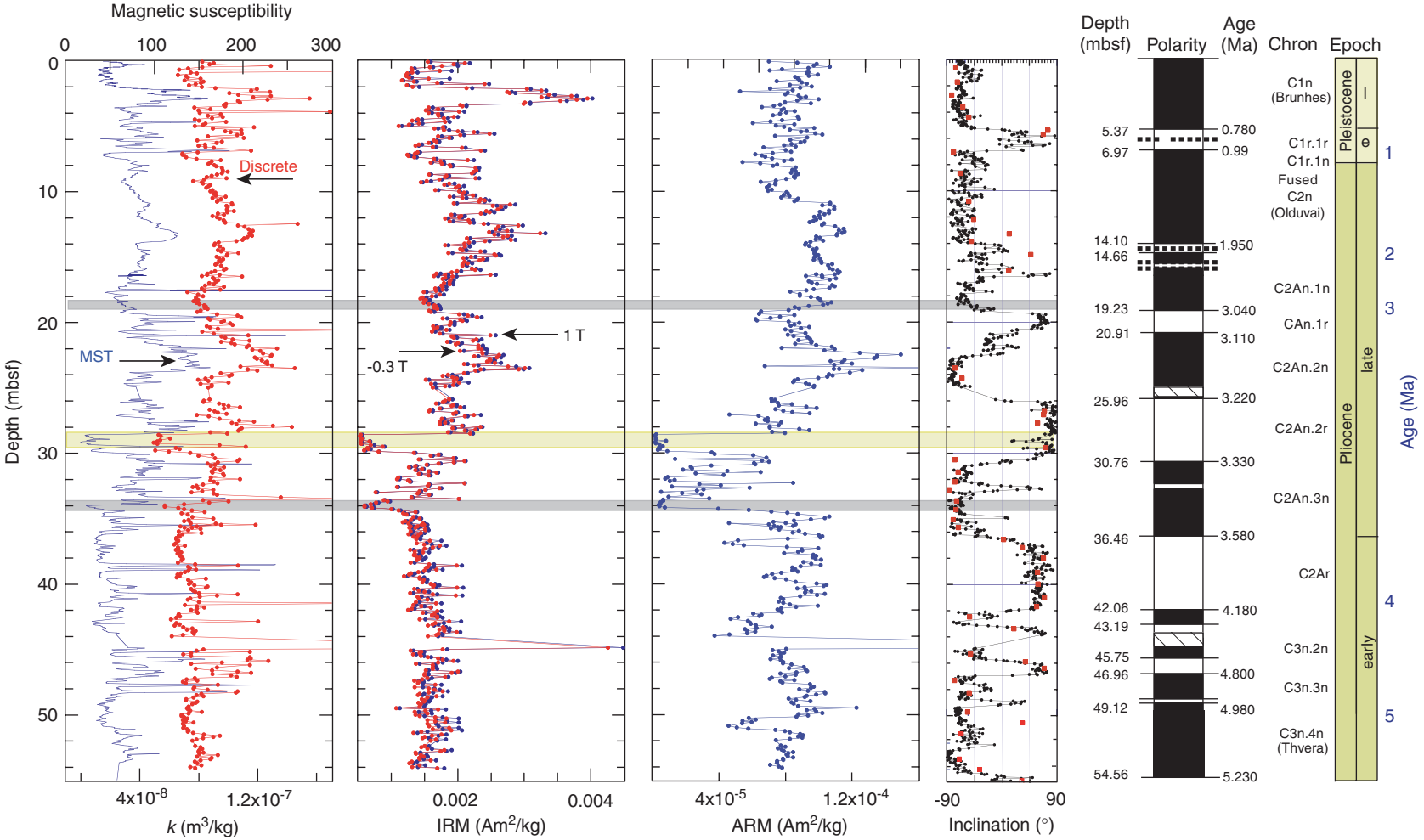

Figure F4. Concentration-independent parameters as a function of stratigraphic depth for the uppermost 54 m at Site 1165. Normalized anhysteretic susceptibility by low-field susceptibility (k_{ARM}/k). Anhysteretic remanent magnetization/isothermal remanent magnetization (ARM/IRM) ratio. S-ratio (IRM[–0.3 T]/IRM[1 T]). (See the **"Supplementary Materials"** contents list for data.)

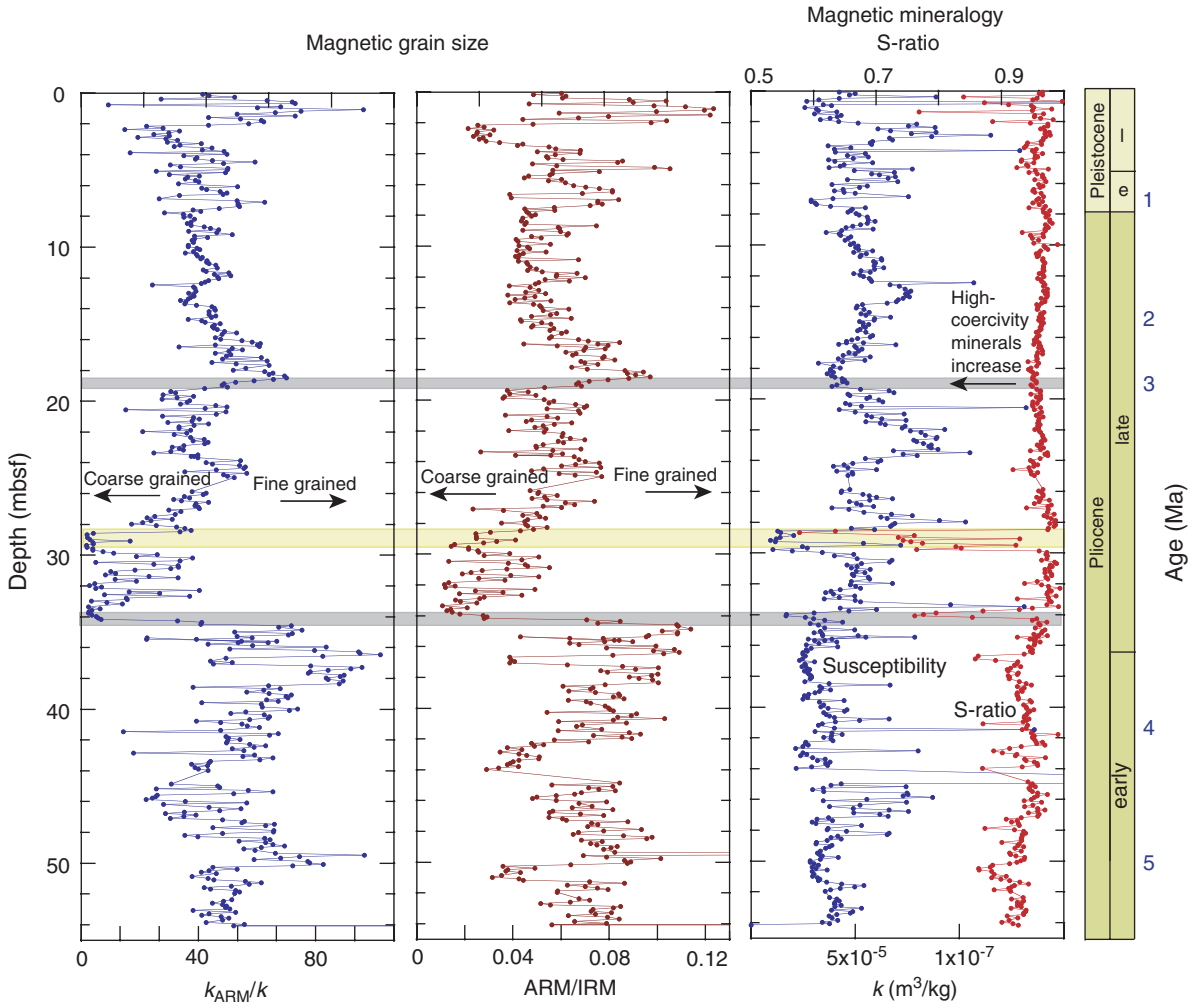

Figure F5. Magnetostratigraphic record from Site 1165 for 0–50 mbsf. The paleomagnetic inclination is shown after demagnetization at 20–30 mT for the split cores (solid line) along with characteristic remanent magnetization (ChRM) data for stepwise-demagnetized discrete samples (open squares). Polarity is shown on the log to the right. Black (white) = normal (reversed) polarity. Marine diatom and radiolarian datums are used to constrain the interpretation. The geomagnetic polarity timescale is from Berggren et al. (1995). (see Fig. F3, p. 22, for data sources)

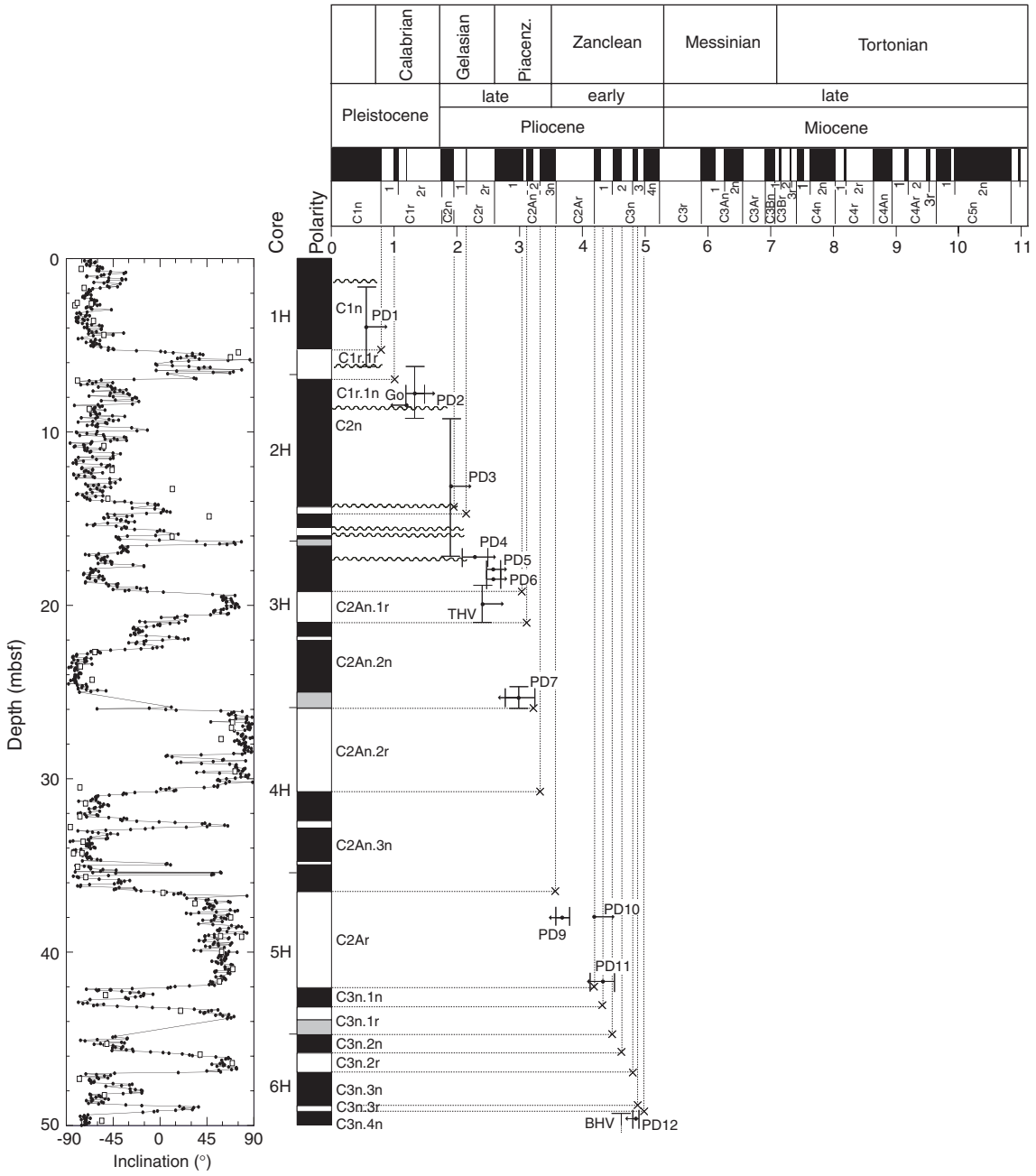

Figure F6. Granulometry of the HiRISC interval. Area below the gravel line is gravel, area below the gravel + sand line is gravel and sand, and remaining area is gravel, sand, and mud. The mud% line is for emphasis only. Note the increase in the sand component above 15 mbsf and particularly above 10 mbsf, signifying the occurrence of foraminifers in the sand-sized fraction. (See the **"Supplementary Materials"** contents list for granulometric data.)

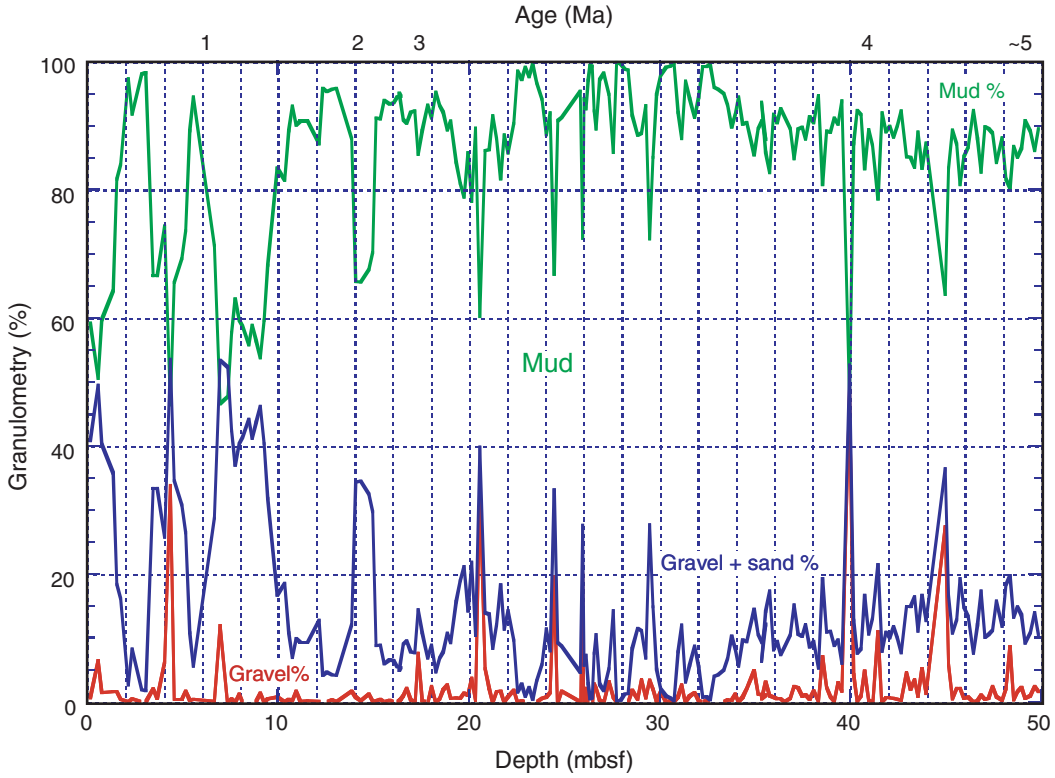

Figure F7. Curves showing changes in brightness down the HiRISC section (0–54 mbsf) of Hole 1165B. The red curve was determined from dry, ground-up core samples using the PerkinElmer Lambda 6 spectrophotometer, whereas the green curve was determined from shipboard measurements on wet cores using the Minolta CM-2002 spectrophotometer (see **Damuth and Balsam,** this volume, their table **T2,** for sample locations and values).

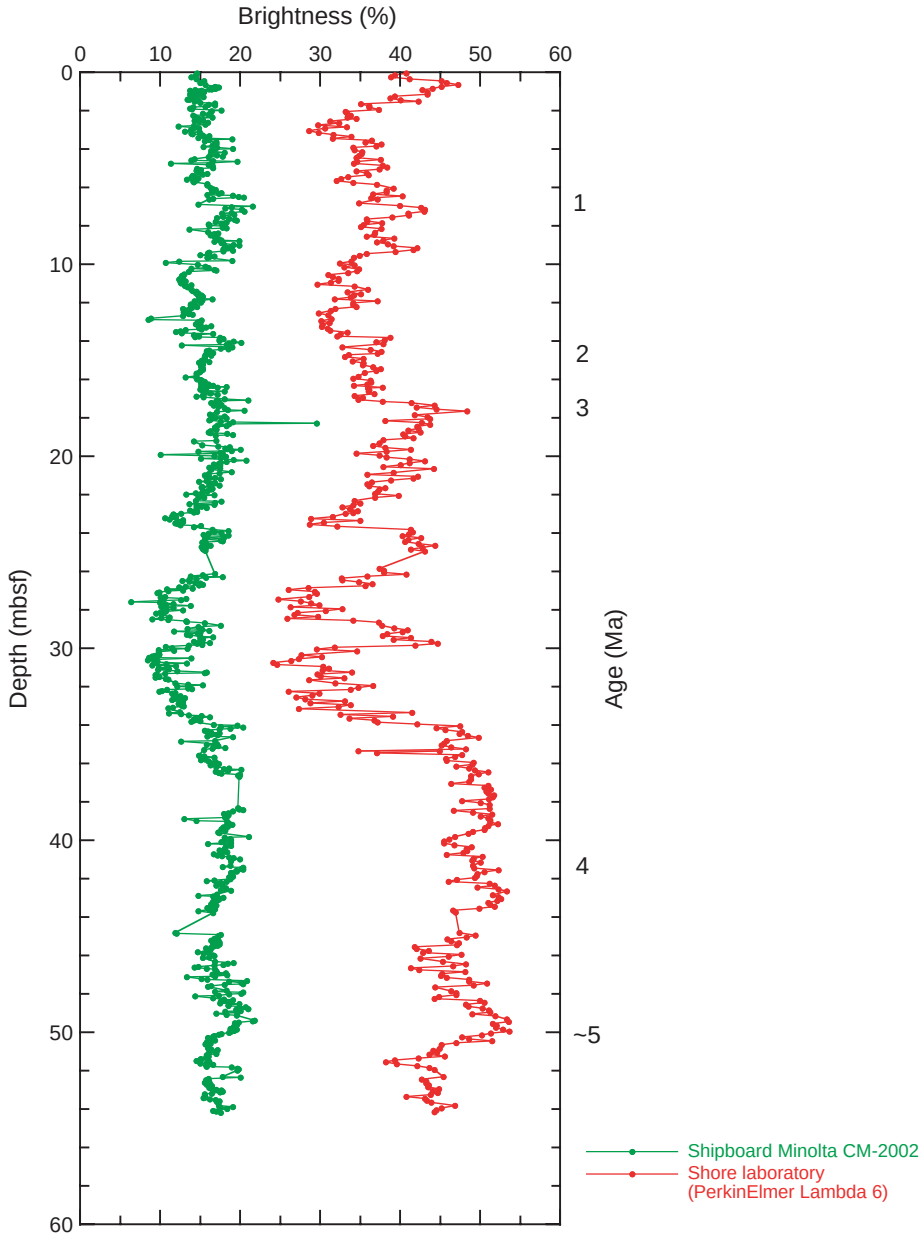

Figure F8. Percent reflectance for six color bands (violet, blue, green, yellow, orange, and red) down the HiRISC section (0–54 mbsf) of Hole 1165B (see **Damuth and Balsam,** this volume, their table **T1,** for sample locations and values).

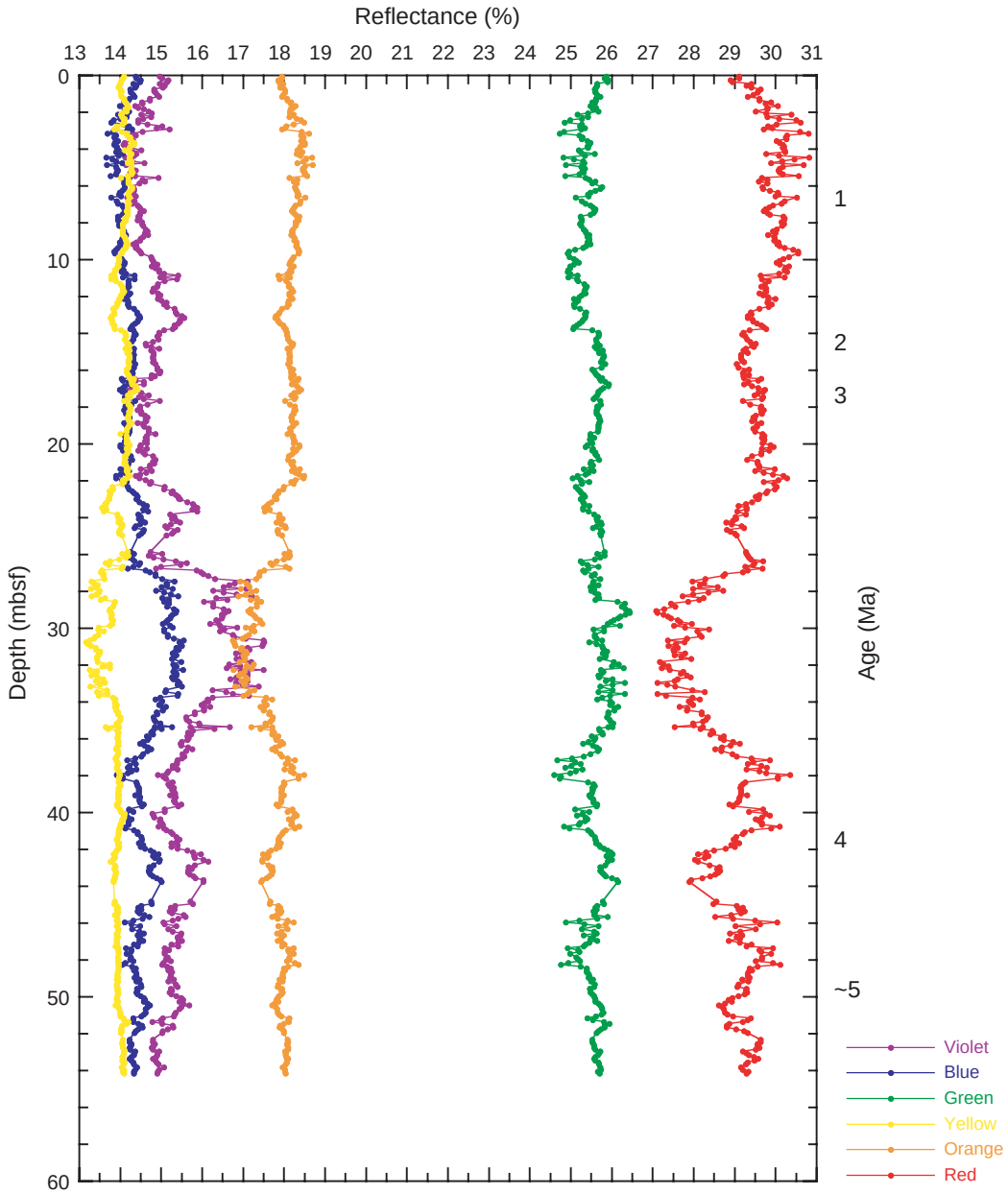

Figure F9. Factor scores for factor 1 (goethite and ripidolite) down the HiRISC section of Hole 1165B (see Damuth and Balsam, this volume, their table T1, for sample locations and values).

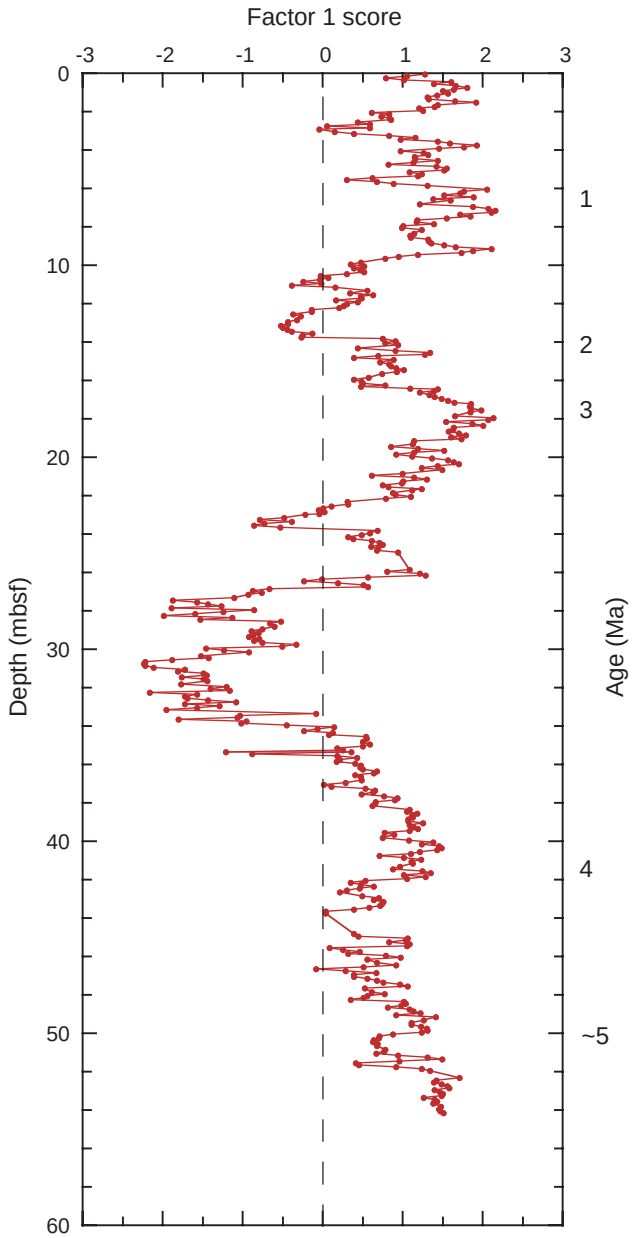

Figure F10. Factor scores for factor 2 (organic matter) down the HiRISC section of Hole 1165B (see **Damuth and Balsam,** this volume, their table **T1,** for sample locations and values).

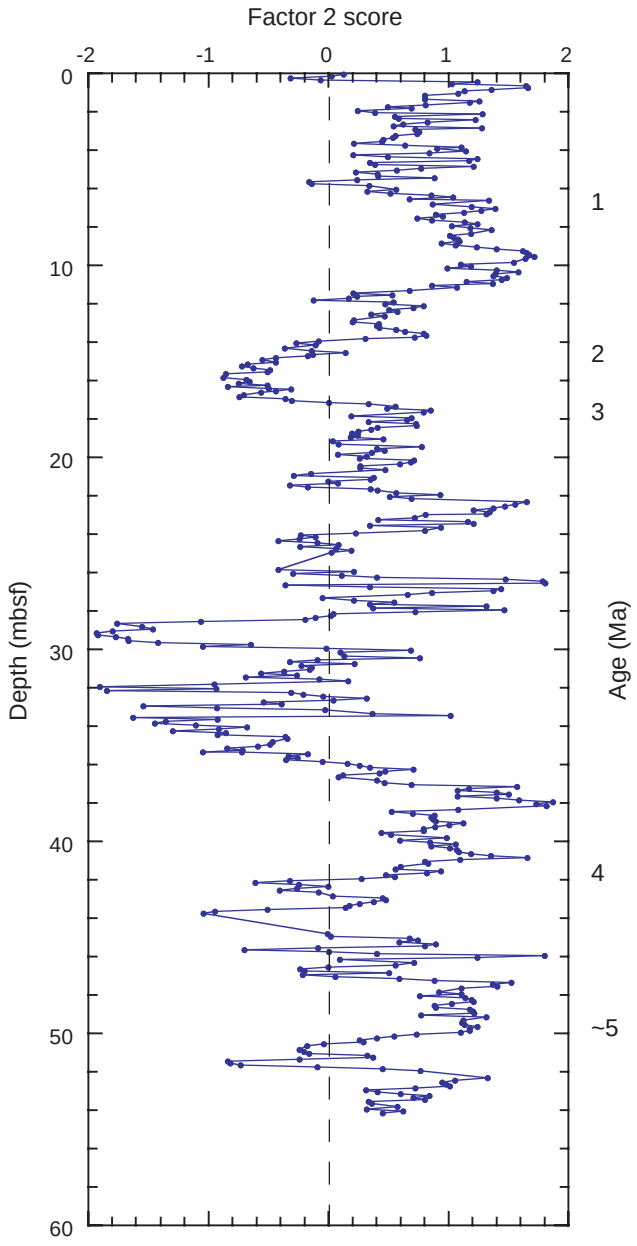

Figure F11. Factor scores for factor 3 (montmorillonite and illite) down the HiRISC section of Hole 1165B (see **Damuth and Balsam,** this volume, their table **T1,** for sample locations and values).

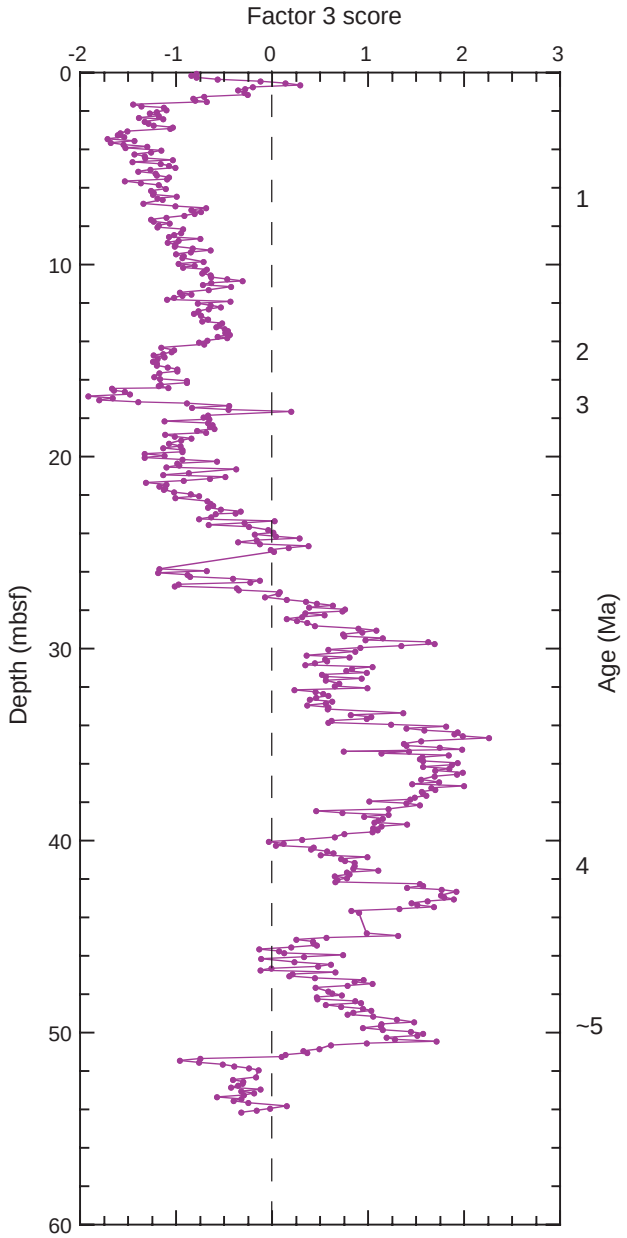

Figure F12. Factor scores for factor 4 (maghemite) down the HiRISC section of Hole 1165B (see **Damuth and Balsam,** this volume, their table **T1,** for sample locations and values).

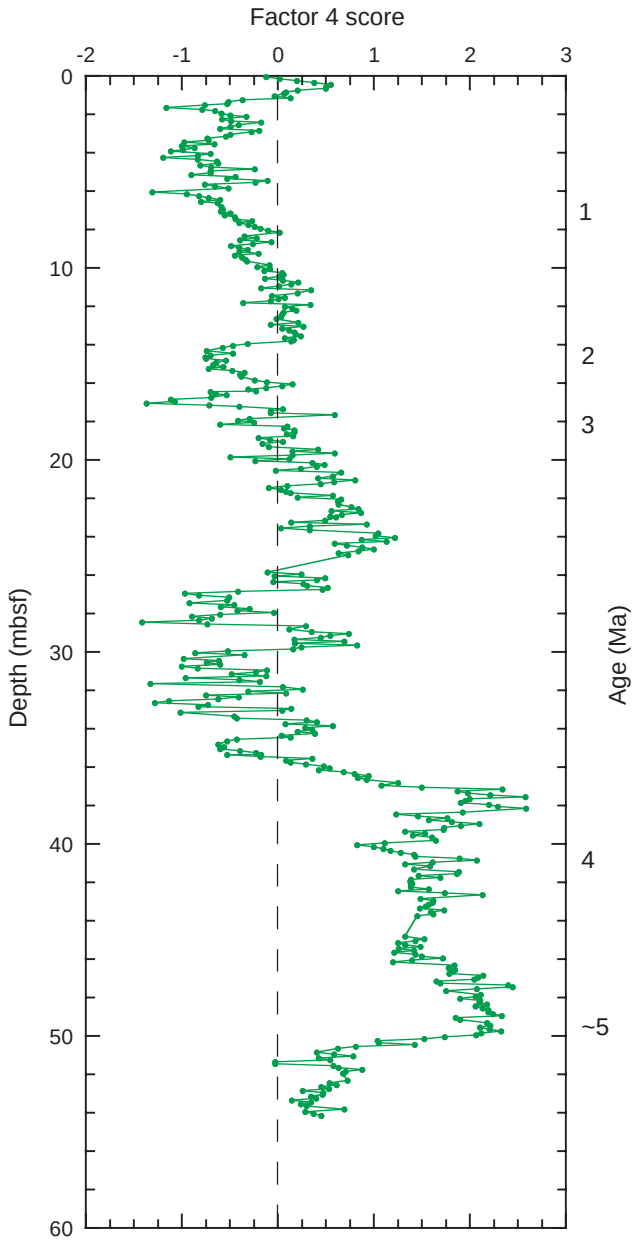

Figure F13. Factor scores for factor 5 (hematite) down the HiRISC section of Hole 1165B (see **Damuth and Balsam,** this volume, their table **T1,** for sample locations and values).

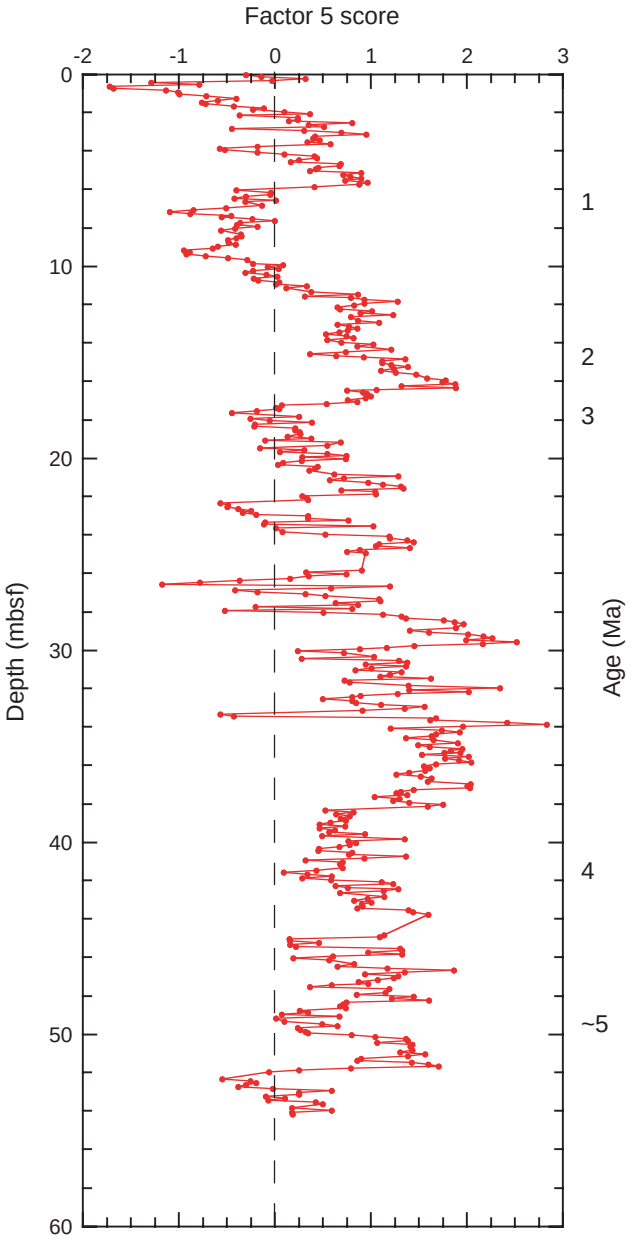

Figure F14. Stable isotopes for the upper HiRISC interval based on *Neogloboquadrina pachyderma* (s). See text for explanation. PDB = Peedee belemnite. (see the **"Supplementary Materials"** contents list for isotopic data.)

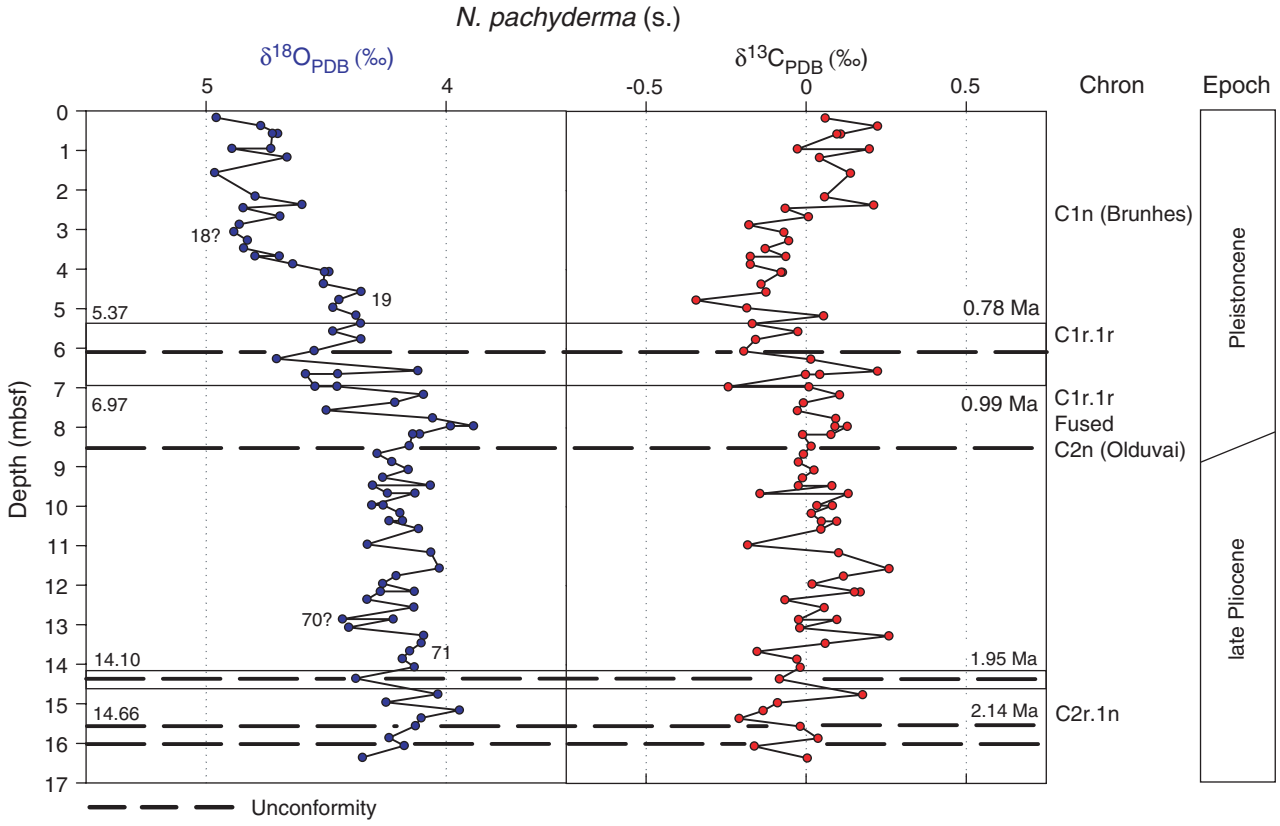

Figure F15. Clay mineral distribution for the HiRISC interval. See text for explanation. (see the **"Supplementary Materials"** contents list for clay mineral data.)

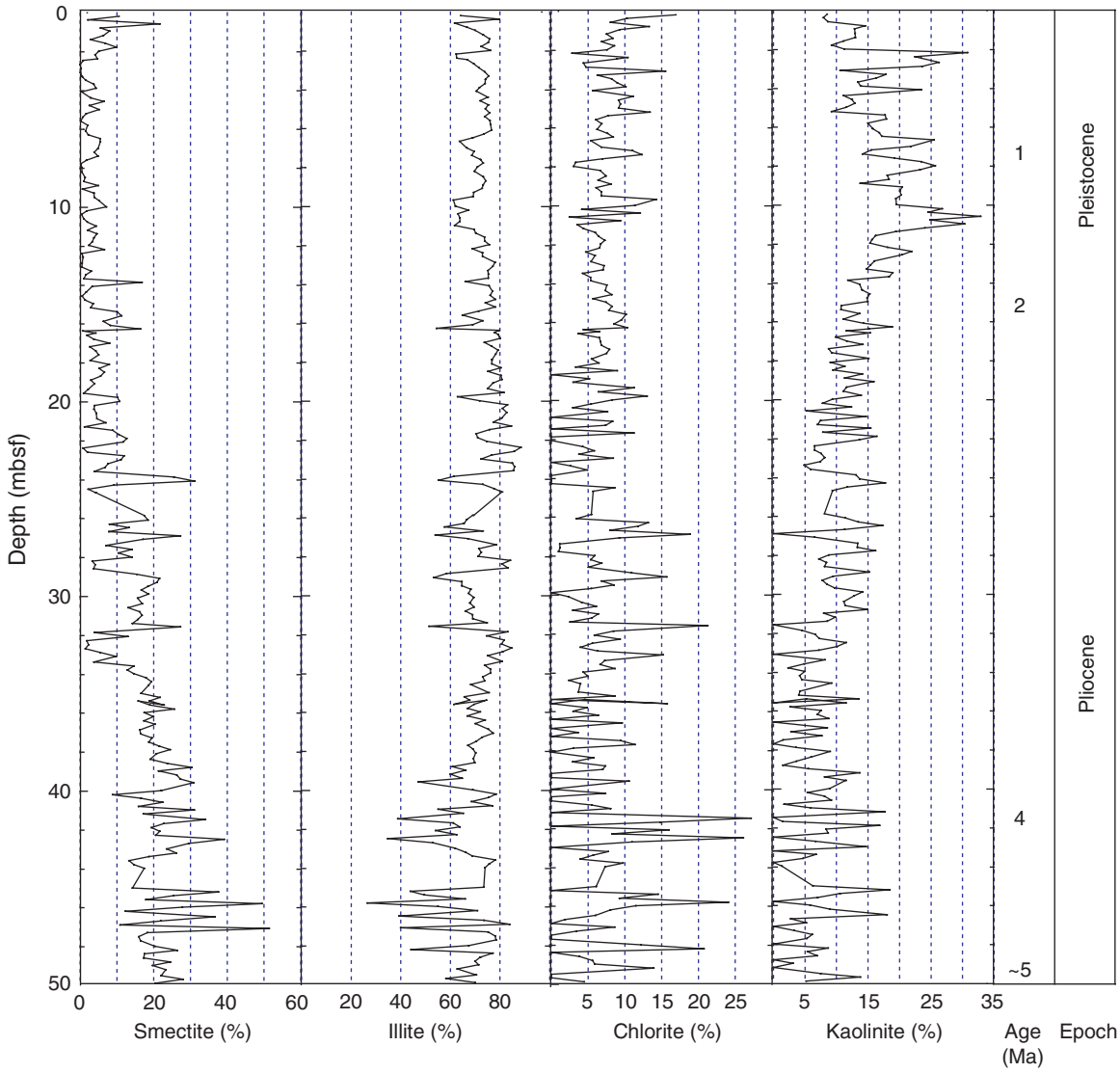

Table T1. List of foraminifers at Site 1165 in the 0- to 15-mbsf interval. (**See table notes.** Continued on next three pages.)

Sample	Core, section, interval (cm)	Depth (mbsf)	Multiple	Total planktonic foraminifers	Total benthic foraminifers	Planktonic (%)	Total foraminifers in sample	Weight (g)	Total foraminifers/g	*Neogloboquadrina pachyderma* (Ehr.)/g	*Alabaminoides exiguus* (Brady)	*Anomalinoides* sp.	*Cassidulinoides* sp.	*Cibicides lobatulus* (Walker and Jacob)	*Cibicides pachyderma* (Rzehak)	*Cibicides subhaidingerii* Parr	*Cyclammina rotundidorsata* (Hantken)	*Dentalina* sp.	*Fissurina* spp.	*Globocassidulina subglobosa* (Brady)	*Gyroidina bradyi* (Trauth)	*Gyroidina broeckhiana* (Karrer)	*Gyroidina soldanii* d'Orbigny	*Gyroidina* sp.	*Lagena hispidula* Cushman	*Lagena* sp.	*Laticarinina pauperata* (Parker and Jones)	*Lenticulina* sp.	*Martinottiella communis* (d'Orbigny)	*Melonis pompilioides* (Fichtel and Moll)	*Osangulariella umbonifera* (Cushman)	*Procerolagena gracillima* (Sequenza)	*Pullenia bulloides* d'Orbigny	*Pullenia quinqueloba* (Reuss)	*Pyrgo* sp.
	188-1165B-																																	
8684	1H-1, 17–21	0.17	64	1,062	15	98.6	70,000	8.91	7,856	7,746	X													X					X	X			X
8686	1H-1, 37–40	0.37	32	606	28	95.6	20,000				X																		X	X				
8688	1H-1, 57–61	0.57	16	148	2	98.7	2,300	4.71	488	482																			X	X				
8690(1)	1H-1, 77–81	0.77	256	1,777	5	99.7	454,000	18.68	123	123	X								X										X	X				
8692	1H-1, 95–100	0.95	16	244	3	98.8	3,900																							X				
8694	1H-1, 117–120	1.17	16	1	0	100	16																											
8696	1H-1, 137–140	1.37	128	1,210	6	99.5	155,000	8.47	18,300	18,208	X															X				X				X
8698	1H-2, 6–9	1.56	16	2	2	50	32	10.17	3	1.5							X											X						
8700	1H-2, 27–30	1.77	8	6	0	100	40	11.14	3.6	3.6																								
8702	1H-2, 47–50.5	1.97	128	799	6	99.2	102,000				X								X										X				
8704	1H-2, 66–71	2.16	16	26	0	100	400	24.39	16	16																								
8706	1H-2, 87–89.5	2.37	8	1	0	100	8	17.45	0.5	0.5																								
8708	1H-2, 95–100	2.45	8	29	0	100	200																											
8710	1H-2, 116.5–120	2.66	16	1	0	100	16																											
8712	1H-2, 137–139.5	2.87	16	34	0	100	500	12.02	42	42																								
8714	1H-3, 6–9	3.06	16	23	0	100	400																											
8716	1H-3, 27–30	3.27	16	40	15	72.3	640				X														X				X	X				
8718	1H-3, 47–49.5	3.47	16	136	20	87.2	2,200	14.01	157	137	X				X				X										X	X				
8720	1H-3, 67–71	3.67	16	31	3	91.2	500	10.06	50	46																				X				
8722	1H-3, 87–89.5	3.87	16	878	22	97.6	12,000				X		X						X									X	X	X	X		
8724	1H-3, 106.5–110	4.07	64	743	6	99.2	47,500	8.64	5,500	5,456	X														X				X			X	
8728	1H-3, 137–140.5	4.37	16	36	12	75	600	9.04	66	49																								
8730	1H-4, 7–9.5	4.57	8	10	17	37	80	13.91	6	2															X					X				
8732	1H-4, 27–30	4.77	64	810	13	98.4	52,000				X								X										X				
8734	1H-4, 47.5–50	4.97	16	19	0	100	300	8.55	35	35																				X				
8736	1H-4, 67–70	5.17	8	1	2	33.3	8	13.02	6	2																								
8738	1H-4, 87–89.5	5.37	8	42	3	93.3	300	11.73	26	24																								
8740	1H-4, 106.5–110	5.57	8	59	4	93.6	500	15.98	31	29									X											X				
8742	1H-4, 127–130	5.77	8	44	19	69.8	400												X											X	X			
8816	1H-5, 6.5–9	6.07	8	44	9	83	400								X															X				
8818	1H-5, 27–29.5	6.27	8	3	0	100	24																											
8820	1H-5, 47.5–50	6.47	64	1,129	15	98.7	72,000				X																			X			X	
8822	1H-5, 65–68	6.65	64	1,202	9	99.3	77,000	10.48	7,347	7,295	X				X			X	X			X												
8824	2H-1, 17–20	6.97	64	1,385	22	98.4	89,000	11.9	7,479	7,359	X				X		X		X						X				X	X		X	X	
8826	2H-1, 37–39.5	7.17	128	2,251	12	99.5	288,000				X				X					X					X					X				X
8828	2H-1, 57–60	7.37	256	1,188	14	98.8	304,000	9.6	31,666	31,286	X				X				X											X			X	
8830	2H-1, 77–80	7.57	128	1,107	10	99.1	142,000	9.19	15,451	15,311	X				X								X	X						X				

Table T1 (continued).

Sample	Core, section, interval (cm)	Depth (mbsf)	Multiple	Total planktonic foraminifers	Total benthic foraminifers	Planktonic (%)	Total foraminifers in sample	Weight (g)	Total foraminifers/g	*Neogloboquadrina pachyderma* (Ehr.)/g	*Siphotextularia concava* (Karrer)	*Siphotextularia* sp.	*Sphaeroidina bulloides* Deshayes	*Trifarina carinata* (Cushman)	*Uvigerina auberiana* d'Orbigny	*Uvigerina brunnensis* Karrer	*Uvigerina canariensis* d'Orbigny	Unidentified benthic foraminifers	Unidentified miliolids	Dominant component	Radiolarians	Accessories	Age (Ma)
	188-1165B-																						
8684	1H-1, 17–21	0.17	64	1,062	15	98.6	70,000	8.91	7,856	7,746			X	X						P	tr	GES	
8686	1H-1, 37–40	0.37	32	606	28	95.6	20,000												X	R	dom.		
8688	1H-1, 57–61	0.57	16	148	2	98.7	2,300	4.71	488	482										R/T	dom.	V	
8690(1)	1H-1, 77–81	0.77	256	1,777	5	99.7	454,000	18.68	123	123		X								P	tr	T	
8692	1H-1, 95–100	0.95	16	244	3	98.8	3,900													T	m	GEV	
8694	1H-1, 117–120	1.17	16	1	0	100	16													T	c	GS	
8696	1H-1, 137–140	1.37	128	1,210	6	99.5	155,000	8.47	18,300	18,208										P		ET	
8698	1H-2, 6–9	1.56	16	2	2	50	32	10.17	3	1.5										R	dom.	AfVS	
8700	1H-2, 27–30	1.77	8	6	0	100	40	11.14	3.6	3.6										T	c	S	
8702	1H-2, 47–50.5	1.97	128	799	6	99.2	102,000													P		GS	
8704	1H-2, 66–71	2.16	16	26	0	100	400	24.39	16	16										T	m	GS	
8706	1H-2, 87–89.5	2.37	8	1	0	100	8	17.45	0.5	0.5										T			
8708	1H-2, 95–100	2.45	8	29	0	100	200													T	m		
8710	1H-2, 116.5–120	2.66	16	1	0	100	16													T	tr	G	
8712	1H-2, 137–139.5	2.87	16	34	0	100	500	12.02	42	42										T	tr		
8714	1H-3, 6–9	3.06	16	23	0	100	400													T		MnG	
8716	1H-3, 27–30	3.27	16	40	15	72.3	640													T	tr	E	
8718	1H-3, 47–49.5	3.47	16	136	20	87.2	2,200	14.01	157	137								X		T	tr	GE	
8720	1H-3, 67–71	3.67	16	31	3	91.2	500	10.06	50	46										T	tr	E	
8722	1H-3, 87–89.5	3.87	16	878	22	97.6	12,000								X			X		PT	tr	E	
8724	1H-3, 106.5–110	4.07	64	743	6	99.2	47,500	8.64	5,500	5,456										P	tr	E	
8728	1H-3, 137–140.5	4.37	16	36	12	75	600	9.04	66	49										T	m	GS	
8730	1H-4, 7–9.5	4.57	8	10	17	37	80	13.91	6	2								X		T	tr	E	
8732	1H-4, 27–30	4.77	64	810	13	98.4	52,000													P	m	ES	
8734	1H-4, 47.5–50	4.97	16	19	0	100	300	8.55	35	35										T	c	E	
8736	1H-4, 67–70	5.17	8	1	2	33.3	8	13.02	6	2										T	r	G	
8738	1H-4, 87–89.5	5.37	8	42	3	93.3	300	11.73	26	24										T	m	G	
8740	1H-4, 106.5–110	5.57	8	59	4	93.6	500	15.98	31	29										T		MnGE	
8742	1H-4, 127–130	5.77	8	44	19	69.8	400													T	c	GEMnS	
8816	1H-5, 6.5–9	6.07	8	44	9	83	400										X			T	m	G	
8818	1H-5, 27–29.5	6.27	8	3	0	100	24													T	m	G*	0.78
8820	1H-5, 47.5–50	6.47	64	1,129	15	98.7	72,000													P	tr	GE	
8822	1H-5, 65–68	6.65	64	1,202	9	99.3	77,000	10.48	7,347	7,295										P		MnGE	
8824	2H-1, 17–20	6.97	64	1,385	22	98.4	89,000	11.9	7,479	7,359	X							X		P		GE	1.77
8826	2H-1, 37–39.5	7.17	128	2,251	12	99.5	288,000													P			
8828	2H-1, 57–60	7.37	256	1,188	14	98.8	304,000	9.6	31,666	31,286						X				P			
8830	2H-1, 77–80	7.57	128	1,107	10	99.1	142,000	9.19	15,451	15,311								X		P		GEMn	

Table T1 (continued).

Sample	Core, section, interval (cm)	Depth (mbsf)	Multiple	Total planktonic foraminifers	Total benthic foraminifers	Planktonic (%)	Total foraminifers in sample	Weight (g)	Total foraminifers/g	*Neogloboquadrina pachyderma* (Ehr.)/g	*Alabaminoides exiguus* (Brady)	*Anomalinoides* sp.	*Cassidulinoides* sp.	*Cibicides lobatulus* (Walker and Jacob)	*Cibicides pachyderma* (Rzehak)	*Cibicides subhaidingerii* Parr	*Cyclammina rotundidorsata* (Hantken)	*Dentalina* sp.	*Fissurina* spp.	*Globocassidulina subglobosa* (Brady)	*Gyroidina bradyi* (Trauth)	*Gyroidina broeckhiana* (Karrer)	*Gyroidina soldanii* d'Orbigny	*Gyroidina* sp.	*Lagena hispidula* Cushman	*Lagena* sp.	*Laticarinina pauperata* (Parker and Jones)	*Lenticulina* sp.	*Martinottiella communis* (d'Orbigny)	*Melonis pompilioides* (Fichtel and Moll)	*Osangulariella umbonifera* (Cushman)	*Procerolagena gracillima* (Sequenza)	*Pullenia bulloides* d'Orbigny	*Pullenia quinqueloba* (Reuss)	*Pyrgo* sp.
8832	2H-1, 97–101	7.77	128	1,414	5	99.6	181,000	7.46	24,263	24,166	X									X	X											X		
8834	2H-1, 117–119.5	7.97	128	919	4	99.6	118,000	6.4	18,438	18,364										X	X											X		
8836	2H-1, 137–140	8.17	64	964	1	99.9	61,000	3.94	15,482	15,467	X																					X		
8838	2H-2, 17–21.5	8.47	128	1,760	4	99.8	224,000	12.52	17,891	17,855	X																					X		X
8840	2H-2, 37–40	8.67	128	169	7	99.6	242,000	12.94	18,701	18,626	X				X				X	X												X		X
8842	2H-2, 57–60	8.87	32	585	1	99.8	18,700	10.64	1,758	1,754																								
8844	2H-2, 77–80	9.07	32	0	1	0	0	9.73	0	0							X																	
8846	2H-2, 97–101	9.27	256	1,169	12	99	297,000	16.29	18,232	18,950	X	X		X					X											X			X	
8848	2H-2, 117–120	9.47	128	1,194	2	99.8	153,000	11.42	13,398	13,371									X								X			X				
8850	2H-2, 137–140	9.67	128	1,412	7	99.5	181,000				X				X															X		X		
8852	2H-3, 17–21	9.97	32	385	5	98.7	12,300	8.57	1,435	1,416		X																		X				
8854	2H-3, 37–40.5	10.17	128	1,360	2	99.8	174,000				X																					X		
8856	2H-3, 57–59.5	10.37	64	920	1	99.9	59,000	12.49	4,724	4,719																								X
8858	2H-3, 77–80	10.57	32	1,201	2	99.8	38,400	12.74	3,014	3,008	X																							
8860	2H-3, 96–100	10.76	16	1,322	4	99.7	21,000	9.42	2,229	2,222	X									X												X	X	
8862	2H-3, 117–119.5	10.97	32	1,564	11	99.3	50,000	13.96	3,582	3,557		X							X							X				X	X	X		
8864	2H-3, 137–139.5	11.17	16	964	3	99.7	15,500	7.36	2,106	2,100	X								X											X				
8914	2H-4, 6–8.5	11.36	32	1,218	2	99.8	39,000				X																			X				
8916	2H-4, 27–29.5	11.57	16	1,116	16	98.6	18,000	14.02	1,284	1,266	X					X			X											X		X		
8918	2H-4, 46–49	11.76	32	1,467	12	99.2	47,000				X																			X		X		X
8920	2H-4, 66–69	11.96	16	863	11	98.7	13,800				X				X										X					X		X		
8922	2H-4, 86–89	12.16	32	660	3	99.5	21,100	18.21	1,159	1,153	X																			X				
8924	2H-4, 106–109	12.36	32	0	0	0	0	17.78	0	0																								
8926	2H-4, 126–128.5	12.56	8	573	7	97.1	4,600	9.4	489	475	X					X			X											X		X	X	
8942	2H-5, 6–8.5	12.86	16	346	1	99.7	5,500	9.07	606	604																				X				
8944	2H-5, 27–29.5	13.07	16	139	0	100	2,200	14.86	13	13																								
8946	2H-5, 47–49.5	13.27	8	321	1	99.7	2,500				X																							
8948	2H-5, 66–69	13.46	4	4	1	80	16																											
8950	2H-5, 86.5–86.9	13.66	4	87	0	100	300																											
8952	2H-5, 106–110	13.86	16	11	4	73.3	200	14.54	14	10						X														X				
8954	2H-5, 117–119.5	13.97	16	8	3	72.7	100	9.9	10	7																				X				
8928	2H-6, 6–8.5	14.36	8	6	3	66.7	48	9.09	5	3																				X				
8930	2H-6, 27–29.5	14.57	16	3	2	60	48																							X				
8932	2H-6, 46–49	14.76	16	1	2	33.3	16	9.44	1.7	0.6																								
8934	2H-6, 66–69	14.96	16	0	0	0	0	9.37	0	0																								

Notes: P = pachyderma dominant, T = terrigenous dominant, P/T = pachyderma dominant over terrigenous, R = radiolarians dominant. Radiolarians: tr = trace, r = rare, m = minor, c = common, dom. = dominant. Accessories: G = glauconite, E = echinoid spines, S = sponge spicules, B = Bone, T = teeth, Mn = Manganese oxides, V = volcanic glass.

Table T1 (continued).

Sample	Core, section, interval (cm)	Depth (mbsf)	Multiple	Total planktonic foraminifers	Total benthic foraminifers	Planktonic (%)	Total foraminifers in sample	Weight (g)	Total foraminifers/g	*Neogloboquadrina pachyderma* (Ehr.)/g	*Siphotextularia concava* (Karrer)	*Siphotextularia* sp.	*Sphaeroidina bulloides* Deshayes	*Trifarina carinata* (Cushman)	*Uvigerina auberiana* d'Orbigny	*Uvigerina brunnensis* Karrer	*Uvigerina canariensis* d'Orbigny	Unidentified benthic foraminifers	Unidentified miliolids	Dominant component	Radiolarians	Accessories	Age (Ma)
8832	2H-1, 97–101	7.77	128	1,414	5	99.6	181,000	7.46	24,263	24,166										P		EMnB	
8834	2H-1, 117–119.5	7.97	128	919	4	99.6	118,000	6.4	18,438	18,364										P		E	
8836	2H-1, 137–140	8.17	64	964	1	99.9	61,000	3.94	15,482	15,467										P		Mn	
8838	2H-2, 17–21.5	8.47	128	1,760	4	99.8	224,000	12.52	17,891	17,855										P		E	
8840	2H-2, 37–40	8.67	128	169	7	99.6	242,000	12.94	18,701	18,626								X		P		Mn	
8842	2H-2, 57–60	8.87	32	585	1	99.8	18,700	10.64	1,758	1,754									X	P/T	tr		
8844	2H-2, 77–80	9.07	32	0	1	0	0	9.73	0	0										T	r	GS	
8846	2H-2, 97–101	9.27	256	1,169	12	99	297,000	16.29	18,232	18,950										P		EMn	1.35–
8848	2H-2, 117–120	9.47	128	1,194	2	99.8	153,000	11.42	13,398	13,371										P		EMn	1.8
8850	2H-2, 137–140	9.67	128	1,412	7	99.5	181,000											X		P	tr	EMn	
8852	2H-3, 17–21	9.97	32	385	5	98.7	12,300	8.57	1,435	1,416										P		Mn	
8854	2H-3, 37–40.5	10.17	128	1,360	2	99.8	174,000													P		MnG	
8856	2H-3, 57–59.5	10.37	64	920	1	99.9	59,000	12.49	4,724	4,719										P		EGT	
8858	2H-3, 77–80	10.57	32	1,201	2	99.8	38,400	12.74	3,014	3,008										P		Mn	
8860	2H-3, 96–100	10.76	16	1,322	4	99.7	21,000	9.42	2,229	2,222										P		E	
8862	2H-3, 117–119.5	10.97	32	1,564	11	99.3	50,000	13.96	3,582	3,557										P		SMn	
8864	2H-3, 137–139.5	11.17	16	964	3	99.7	15,500	7.36	2,106	2,100										P		EMn	
8914	2H-4, 6–8.5	11.36	32	1,218	2	99.8	39,000													P		E	
8916	2H-4, 27–29.5	11.57	16	1,116	16	98.6	18,000	14.02	1,284	1,266										T/P		EMn	
8918	2H-4, 46–49	11.76	32	1,467	12	99.2	47,000													P/T		ES	
8920	2H-4, 66–69	11.96	16	863	11	98.7	13,800											X		T/P		GEMn	
8922	2H-4, 86–89	12.16	32	660	3	99.5	21,100	18.21	1,159	1,153			X							P/T		E	
8924	2H-4, 106–109	12.36	32	0	0	0	0	17.78	0	0										T	m		
8926	2H-4, 126–128.5	12.56	8	573	7	97.1	4,600	9.4	489	475										T/P		E	
8942	2H-5, 6–8.5	12.86	16	346	1	99.7	5,500	9.07	606	604										PT	tr		
8944	2H-5, 27–29.5	13.07	16	139	0	100	2,200	14.86	13	13								X		T/P			
8946	2H-5, 47–49.5	13.27	8	321	1	99.7	2,500													T/P			
8948	2H-5, 66–69	13.46	4	4	1	80	16											X		T	tr	Mn	*G. pu.*
8950	2H-5, 86.5–86.9	13.66	4	87	0	100	300													T	tr	Mn	
8952	2H-5, 106–110	13.86	16	11	4	73.3	200	14.54	14	10								X		T	c	E	
8954	2H-5, 117–119.5	13.97	16	8	3	72.7	100	9.9	10	7										T	tr	S	
8928	2H-6, 6–8.5	14.36	8	6	3	66.7	48	9.09	5	3										T	tr	EMn	1.95
8930	2H-6, 27–29.5	14.57	16	3	2	60	48													T	tr	G	
8932	2H-6, 46–49	14.76	16	1	2	33.3	16	9.44	1.7	0.6								X		T	tr	S	2.14
8934	2H-6, 66–69	14.96	16	0	0	0	0	9.37	0	0										T	tr		